# COMPRESSION RATIO AND CATALYST AGING EFFECTS ON AQUEOUS ETHANOL IGNITION (YEAR 2)

**Final Report**

**KLK756**

**Part 2 Catalyst Aging and Effects of Water on Ignition**

**N09-12**


**National Institute for Advanced Transportation Technology**

**University of Idaho**

**Katrina Leichliter, Dr. Judi Steciak,**

**Dr. Steve Beyerlein, Dr. Ralph Budwig**


**September 2009**

## DISCLAIMER

| | | |
|---|---|---|
| 1. Report No. | 2. Government Accession No. | 3. Recipient's Catalog No. |
| 4. Title and Subtitle<br>Compression Ratio and Catalyst Aging Effects on Aqueous Ethanol Ignition (Year 2): Part 2. Catalyst Aging and Effects of Water on Ignition | | 5. Report Date<br>September 2009<br>6. Performing Organization Code<br>KLK756 |
| 7. Author(s)<br>Leichliter, Katrina; Steciak, Dr. Judi; Beyerlein, Dr. Steve; Budwig, Dr. Ralph | | 8. Performing Organization Report No.<br>N09-12 |
| 9. Performing Organization Name and Address<br>National Institute for Advanced Transportation Technology<br>University of Idaho<br>PO Box 440901; 115 Engineering Physics Building<br>Moscow, ID 838440901 | | 10. Work Unit No. (TRAIS)<br>11. Contract or Grant No.<br>*DTRT07-G-0056* |
| 12. Sponsoring Agency Name and Address<br>US Department of Transportation<br>Research and Special Programs Administration<br>400 7th Street SW<br>Washington, DC 20509-0001 | | 13. Type of Report and Period Covered<br>Final Report: August 2008 – September 2009<br>14. Sponsoring Agency Code<br>*USDOT/RSPA/DIR-1* |
| 15. Supplementary Notes: | | |

16. Abstract

A tubular plug-flow reactor under low Reynolds Numbers $R_e$ flow regimes, along with a 127 μm diameter coiled platinum (Pt) wire, were used to study catalytic surface reactions of nonflammable, fuel-lean mixtures of propane, oxygen, and water vapor diluted with nitrogen. The average wire temperature at ignition, the power required to initiate surface reactions, and the power generated from surface reactions were calculated from experimental data.

Ignition temperatures varied from 450 to 540 K +/- 1 K and heat generation flux varied from 6 to 11.2 W/cm$^2$ depending on the fuel, oxygen and water content. Less than 6 W/cm$^2$ electrical flux to the wire was required to initiate surface reactions.

Aging effects were observed. Unseasoned wires had to be heated to a higher temperature before surface reactions occurred. Grain growth was observed in seasoned wires. Eventually, catalyst performance suffered and deposits were seen at grain edges.

Water vapor affected the combustion process, but not as much as was expected at the fuel:water ratio used (maximum 70:30 propane:water molar ratio). The ignition temperatures of wet experiments increased by no more than 10 K. Water had little effect on the heat generated due to surface reactions with at most ~3% difference between dry and wet experiments.

The finite volume modeling program Fluent® was used to predict the average wire temperature as a function of power input to the wire in air cross-flow. These results were within ~25 K of the values calculated from experimental data.

| | |
|---|---|
| 17. Key Words<br>Pollutant control, fuel systems, engine testing, renewable fuels | 18. Distribution Statement<br>Unrestricted; Document is available to the public through the National Technical Information Service; Springfield, VT. |

| | | | |
|---|---|---|---|
| 19. Security Classif. (of this report)<br>Unclassified | 20. Security Classif. (of this page)<br>Unclassified | 21. No. of Pages<br>61 | 22. Price<br>… |

Form DOT F 1700.7 (8-72) Reproduction of completed page authorized

## Table of Contents

List of Figures ..... iii
List of Tables ..... iv
Nomenclature ..... v
1 Introduction ..... 1
1.1 Background and Motivation ..... 1
1.2 Objective and Outline ..... 2
2 Experimental Apparatus and Experimental Methods ..... 4
2.1 Apparatus ..... 5
2.2 Methods ..... 12
3 Experimental Results ..... 18
3.1 Average Wire Temperature vs. Power ..... 18
3.2 Ignition Temperature and Surface Reaction Energy Generation Calculations ..... 26
3.3 Effect of Water Addition ..... 33
4 Heat Transfer Modeling ..... 39
4.1 Fluent® Finite Volume Analysis ..... 39
4.1.1 Methods ..... 39
4.1.2 Results ..... 47
4.2 Partial Differential Equation Model ..... 50
4.3 Results of Heat Transfer Modeling ..... 52
5 Conclusions and Future Work ..... 56
5.1 Conclusions ..... 56
5.2 Future Work ..... 57
6 References ..... 58

## List of Figures

Figure 2-1: Flammability limits for propane-air mixtures diluted with nitrogen [15]..... 5
Figure 2-2: Water injection cross section view..... 6
Figure 2-3: Sintered metal filter wicking liquid from a pool..... 6
Figure 2-4: Experimental schematic to verify steady flow of expected water vapor content... 7
Figure 2-5: Water injection into gas stream..... 8
Figure 2-6: Example of output humidity ratio data from dew point monitor. ..... 8
Figure 2-7: Experimental schematic for ignition temperature data collection. ..... 11
Figure 2-8: T vs. power curve for air flow over the wire with experimental uncertainty. ..... 12
Figure 2-9: Calculating $Q_{gen}$, the heat generation from reactions on the catalyst surface. ..... 15
Figure 2-10: T and power input vs. time with a constant current input..... 17
Figure 3-1: Average wire temperature vs. power for 1.5% fixed propane, dry..... 20
Figure 3-2: Average wire temperature vs. power for 1.5% fixed propane, 30% water. ..... 21
Figure 3-3: Average wire temperature vs. power for 12.5% fixed oxygen, dry. ..... 22
Figure 3-4: Average wire temperature vs. power for 12.5% fixed oxygen, 40% water. ..... 23
Figure 3-5: Wire temperature vs. current for a 'seasoned' wire compared to a 'fresh' wire [3].24
Figure 3-6: Temperature vs. Power for 5% $O_2$ on two different dates. ..... 25
Figure 3-7: Unseasoned Pt wire showing small grain boundaries and inclusions..... 25
Figure 3-8: Seasoned Pt wire with grain boundary growth and deposits on reaction sites. ... 26
Figure 3-9: Summary of ignition temperatures for fixed volume dry propane mixtures..... 28
Figure 3-10: Summary of ignition temperatures for fixed volume dry oxygen mixtures..... 29
Figure 3-11: Summary of $Q_{gen}$ for fixed volume dry propane mixtures..... 30
Figure 3-12: Summary of $Q_{gen}$ for fixed volume dry oxygen mixtures. ..... 31
Figure 3-13: Equivalence ratio vs. $T_{ig}$ comparison at 7.5% fixed volume of oxygen. ..... 32
Figure 3-14: Impact of water on $T_{ign}$ for 1.5% fixed volume propane. ..... 34
Figure 3-15: Impact of water on $T_{ign}$ for 12.5% fixed volume oxygen. ..... 35
Figure 3-16: Impact of water on $Q_{gen}$ for 1.5% fixed volume propane..... 36
Figure 3-17: Impact of water on $Q_{gen}$ for 12.5% fixed volume oxygen..... 37
Figure 4-1: Platinum coil in the quartz tube, glowing from electrical heating. ..... 41
Figure 4-2: Gambit® mesh for preliminary model, 237,107 elements..... 41

Figure 4-3: Gambit® mesh for detailed model, 312,189 elements. ..... 41
Figure 4-4: Fluent® velocity contours around the electrically heated platinum coil. ..... 46
Figure 4-5: Velocity profiles near the coil measured with a hot-wire anemometer. ..... 47
Figure 4-6: Coiled wire and flow temperature contours with power set to 9 W. ..... 48
Figure 4-7: Temperature distribution of the coiled wire with power set to 9 W. ..... 49
Figure 4-8: Experimental data with Fluent® preliminary and detailed model results..... 49
Figure 4-9: 3-D mesh, temperature vs. time vs. position along wire. ..... 52
Figure 4-10: Steady-state temperature profile along wire length. ..... 52
Figure 4-11: Summary of experimental data and results from the Fluent® and PDE models.55

## List of Tables

Table 2.1: Experimental Uncertainty due to SourceMeter Accuracy ..... 10
Table 3.1: Experiment Matrix ..... 19
Table 4.1: Summary of Material Property Settings ..... 43
Table 4.2: Summary of Boundary Condition Settings ..... 44
Table 4.3: Summary of Model Settings ..... 45
Table 4.4: Average Temperature Experimental Data and Heat Transfer Models Results..... 53

## Nomenclature

| | | |
|---|---|---|
| $C_p$ | Specific heat | (J/kg·K) |
| CPT | Catalytic Plasma Torch | (-) |
| d | Quartz tube inner diameter | (m) |
| D | Catalyst wire diameter | (m) |
| g | Gravity | ($m/s^2$) |
| h | Convection coefficient | ($W/m^2 \cdot K$) |
| HCCCI | Homogeneous charge catalytically assisted compression ignition | (-) |
| I | Current | (A) |
| $k_t$ | Thermal conductivity of the gas | (W/m·K) |
| L | Wire length | (m) |
| $MW_i$ | Molecular weight of species *i* | (kg/kmol) |
| n | Index of refraction | (-) |
| Nu | Nusselt number | (-) |
| P | Power | (W) |
| $P_{ign}$ | Power at catalytic ignition | (W) |
| Pr | Prandlt number | (-) |
| $p$ | Pressure | (Pa) |
| $p_i$ | Partial pressure of species *i* | (Pa) |
| $Q_e$ | Electric energy input to the wire | (W) |
| $Q_{gen}$ | Energy generation from surface reactions | (W) |
| R | Resistance at any temperature T | (Ω) |
| $R_e$ | Reynolds number | (-) |

| | | |
|---|---|---|
| $R_g$ | Universal gas constant | (kJ/kmol·K) |
| r | Radial coordinate in Navier-Stokes equation | (m) |
| $R_i$ | Ideal gas constant of species *i* | (kJ/kmol·K) |
| RMS | Root mean square | (-) |
| ST | Source term in PDE (divided by $\rho \cdot C_p$) | (K/s) |
| t | Time | (s) |
| T | Temperature | (K) |
| $T_{ign}$ | Temperature at catalytic ignition | (K) |
| U | Internal energy storage | (J) |
| v | Velocity | (m/s) |
| $\forall$ | Volume | ($m^3$) |
| V | Voltage | (V) |
| $w_r$ | Water to propane volume ratio, $x_{H_2O}/(x_{H_2O} + x_{C_3H_8})$ | (-) |
| $x_i$ | Mole or volume fraction of species *i* | (-) |
| *z* | Polar angle in Navier-Stokes equation | (°) |

**Greek**

| | | |
|---|---|---|
| α | Temperature coefficient of resistance | (1/K) |
| $\alpha_d$ | Diffusivity | ($m^2$/s) |
| β | Coefficient for convection term in PDE | (1/s) |
| γ | Coefficient for radiation term in PDE | (1/s·$K^3$) |
| ε | Emissivity | (-) |
| θ | Angular coordinate in Navier-Stokes equation | (°) |
| μ | Dynamic viscosity | (kg/m·s) |
| ν | Kinematic viscosity | ($m^2$/s) |

| | | |
|---|---|---|
| $\rho$ | Density | $(kg/m^3)$ |
| $\sigma$ | Stefan-Boltzmann constant | $(W/m^2 \cdot K^4)$ |
| $\varphi$ | Modified equivalence ratio | (-) |
| $\Phi$ | Energy generation within a solid | $(W/m^3)$ |
| $\omega$ | Reaction rate | $(kmol/m^2 \cdot s)$ |

**Subscripts**

| | |
|---|---|
| F | Fuel |
| $O_2$ | Oxygen |
| Pt | Platinum |

# 1 Introduction

The purpose of this project was to study the effects of propane-oxygen-water vapor mixtures, diluted with nitrogen, over a coiled platinum wire catalyst continually exposed to heterogeneous reactions without cleaning. The experimental data has been used to validate a Fluent® finite volume model of the catalyst. The data obtained from this research will be useful in continued development of homogeneous charge, catalytically assisted compression ignition engines (HCCCI).

A tubular plug-flow reactor was used under low Reynolds Number ($R_e$) flow to study the interaction of propane-oxygen mixtures over a seasoned platinum catalyst [1]. The reactor was first tested to ensure plug-flow had been achieved. Then, ignition temperature data was collected for nonflammable propane-oxygen mixtures over 127µm and 203 µm platinum catalyst wires. This data was then compared to that of Cho and Law [2] which verified the experimental apparatus and methods were accurate, Lounsbury [3]. With the method's accuracy confirmed, other fuels could be tested with confidence. However, before continuing with alternative fuels, some adjustments were made to the apparatus and methods to increase the repeatability of experiments as well as the quality of the data collected. With these improvements in place, experiments with the dry mixtures of propane, oxygen and nitrogen were repeated, giving results similar to those from Lounsbury [3]. Ignition temperature, power at ignition, and surface heat generation were then found for the propane-oxygen-nitrogen mixtures with water vapor added. Generally, the water vapor hindered the combustion process, as was expected, increasing both the ignition temperature and power required for ignition, but had little effect on the heat generated due to surface reactions. This work improved the basis laid down by Lounsbury [3] to further research ignition properties of alternative fuels, specifically the effect of water addition in fuels such as ethanol.

## 1.1 Background and Motivation

To investigate heterogeneous reactions on a catalyst, a tubular plug-flow reactor was constructed as outlined in [1]. Experiments were run to collect ignition data of propane-air mixtures over a platinum catalyst and the results were compared to previous research [2] to validate the experimental setup [3]. The next task was to add water vapor to the fuel mixtures

and document the effects on the ignition data. This research will continue with experiments using ethanol and ethanol-water mixtures over the catalyst to further develop a catalytic plasma torch (CPT) igniter or SmartPlug®. The SmartPlug® is designed for HCCCI and uses an in-cylinder platinum/rhodium catalyst within a small pre-chamber adjacent to the main combustion chamber to ignite aqueous ethanol (aquanol) mixtures [4-6]. The University of Idaho has a long-standing research interest in HCCCI of aqueous ethanol. Previous research has shown potential of catalytic ignition of lean aqueous fuel mixtures to reduce harmful emissions and increase engine efficiency over conventional engine configurations.

## 1.2 Objective and Outline

The purpose of this study was to determine what effects adding water to fuel-air mixtures has on heterogeneous reactions on a seasoned platinum wire and to attempt to model the results. The experimental setup was designed to give surface reaction data similar to the response of the CPT igniter in an internal combustion engine. The power input to the catalyst necessary to initiate surface reactions, as well as the ignition temperature and energy generation due to surface reactions, are valuable in further improving the CPT design and ignition timing models. For example, during cold start electrical power must be supplied to raise the surface of the CPT core to ignition temperature. Once the engine is warm, heat generation due to surface reactions sustains repeated ignition and electrical power is no longer required. Ignition timing is affected by the electrical power supplied, the core temperature reached, and by heat generation.

A Fluent® finite volume model was applied to the data. The Fluent® model will be used to predict ignition temperatures and surface heat generation once it is integrated with Chemkin®.

The experimental apparatus and methods used to collect the ignition temperature and heat release data is outline in Chapter 2. Chapter 3 summarizes and discusses the experimental results for average wire temperatures as a function of power input, ignition temperatures, and energy generation due to surface reactions, depending on the fuel mixture. Chapter 4 discusses the heat transfer models applied to the system, the Fluent® finite volume model as

well as an analytical partial differential equation model of the catalyst. Lastly, Chapter 5 summarizes findings and suggestions for future work.

## 2 Experimental Apparatus and Experimental Methods

This chapter describes the experimental setup and methods used to measure and calculate the ignition temperatures and heat generation on the platinum surface of the propane-oxygen-water mixtures. A tubular plug flow reactor was designed and calibrated using a hot-wire anemometer as described by Lounsbury [3]. It was determined that the reactor achieved plug-flow conditions at approximately 3-11 diameters downstream from the nozzle. To ensure constant velocity across the quartz reactor exhaust tube the catalyst was placed at approximately 7 diameters downstream of the nozzle.

All experiments were performed with non-flammable mixtures of propane, oxygen, nitrogen, and some included water vapor, each with a total flow rate of 5 $^{L}/_{min.}$. Figure 2-1 Lewis and Von Elbe[15] show that mixtures with less than 2% propane or less than 12% oxygen, by volume, can be considered non-flammable. In this study, data was collected for fixed volume percentages of oxygen, from 5% ≤ $x_{O_2}$ ≤ 20% in 2.5% increments, and for fixed volume percentages of propane, from 1% ≤ $x_{C_3H_8}$ ≤ 2% in 0.5% increments. Each of these data sets were also run with water vapor added as a fixed volume ratio to propane, from 10% ≤ $x_{H_2O}/(x_{H_2O} + x_{C_3H_8})$ ≤ 40% in 10% increments. For these experiments, a modified equivalence ratio, φ, was defined as the ratio of the mass of propane to oxygen divided by an equivalent stoichiometric ratio. Each data set was run through an equivalence ratio from 0.1 ≤ φ ≤ 1.0 in 0.1 increments. Hence, the impact of both the relative (via φ) and absolute values of fuel and oxygen on $T_{ig}$ and $Q_{gen}$ were obtained.

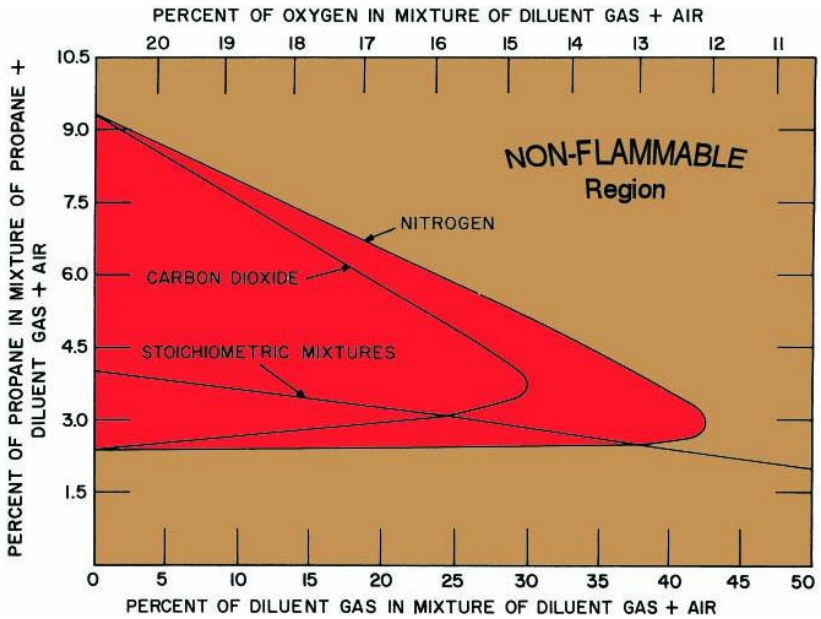


**Figure 2-1: Flammability limits for propane-air mixtures diluted with nitrogen [15].**

## 2.1 Apparatus

All experiments were run controlling the equipment from the lab computer using LabView®. There were two experimental set ups. The first was used to verify steady flow of the expected water content and the second to take ignition temperature data.

Figure 2-4 shows the experimental setup used while verifying the water content in the flow stream. Nitrogen was metered through the Porter mass flow controller and controlled with an NI-9263 analog out CompacDAQ. Before and after the water was injected into the nitrogen stream, the gas passed through a heating coil constructed of $^{1}/_{8}$ inch stainless steel tubing wrapped with two Amptek electrical heating tapes. Each of these heating tapes was controlled with a variable voltage power supply, one ranging from 0-156 W and the other ranging from 0-104 W. At the injection site, the gas stream flowed over a stainless steel sintered metal wick that the Yale Apparatus syringe pump pushed water through as illustrated in Figure 2-2. Figure 2-3 shows a close view of the sintered metal filter in a pool of liquid to display its wicking capability. For these experiments, a $^{1}/_{8}$ inch diameter by $^{1}/_{8}$ inch long stainless steel filter with a filter size of 100 microns was used. The syringe pump, power supplies, and heating coil are shown in Figure 2-5. After the gas and vapor mixture left the heating coil, which hopefully evaporated any remaining liquid droplets from the

wick, it entered the hygrometer where the dew point was measured and sent to the computer through the Keithley® SourceMeter. An example of the humidity ratio output data is shown in Figure 2-6. Results clearly show that as the water content becomes increasingly less steady above a flow rate of approximately 1000 $^{\mu L}/_{min}$.

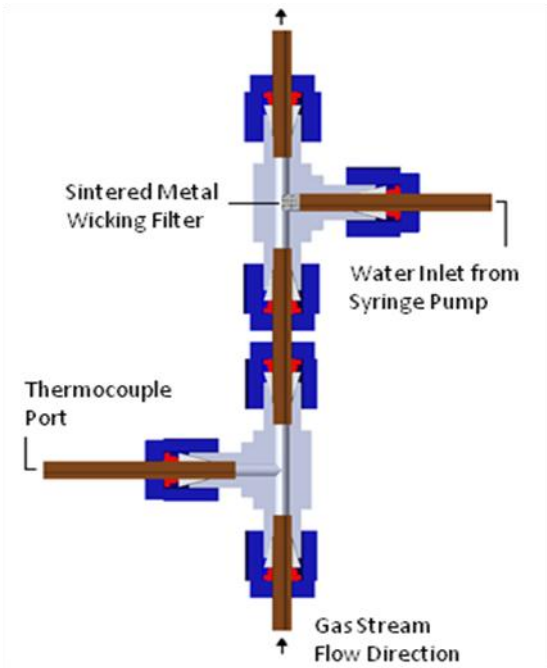


**Figure 2-2: Water injection cross section view.**

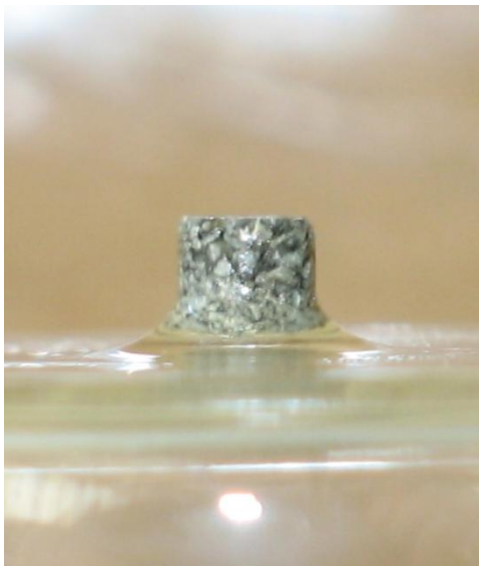

**Figure 2-3: Sintered metal filter wicking liquid from a pool.**

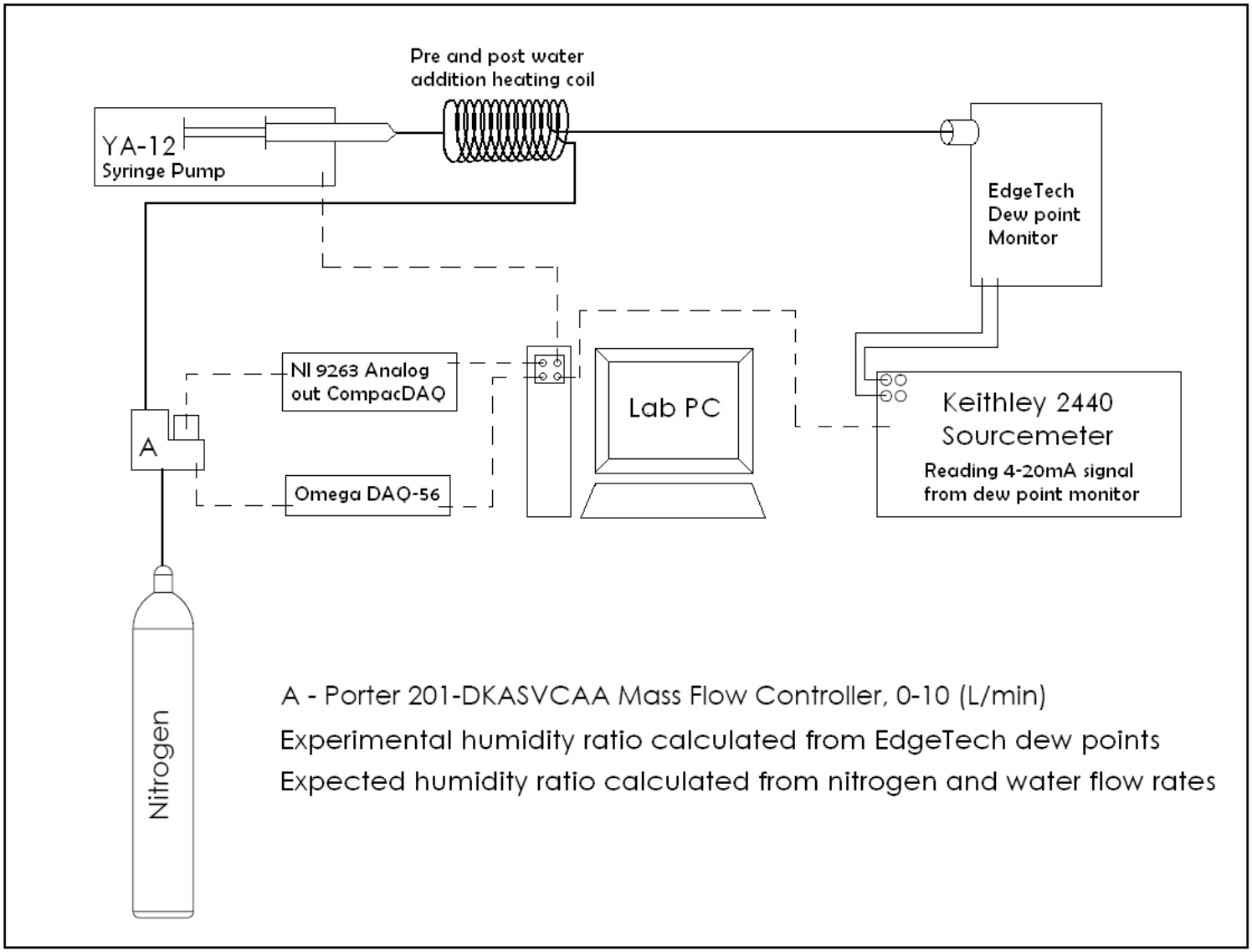


**Figure 2-4: Experimental schematic to verify steady flow of expected water vapor content.**

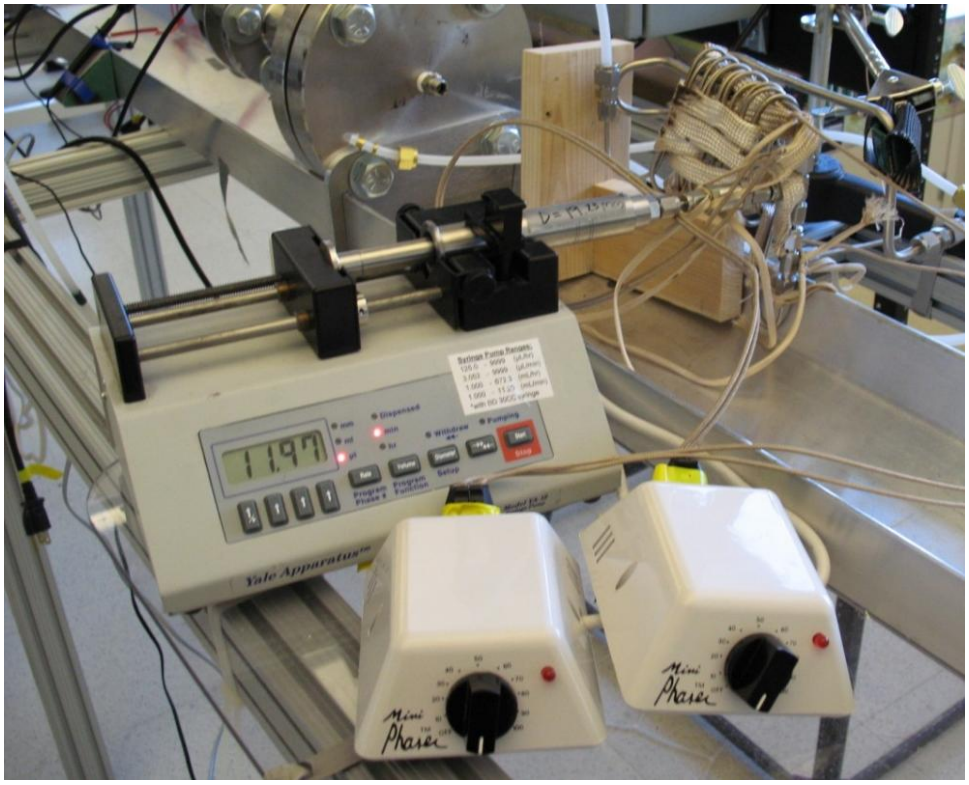


**Figure 2-5: Water injection into gas stream.**

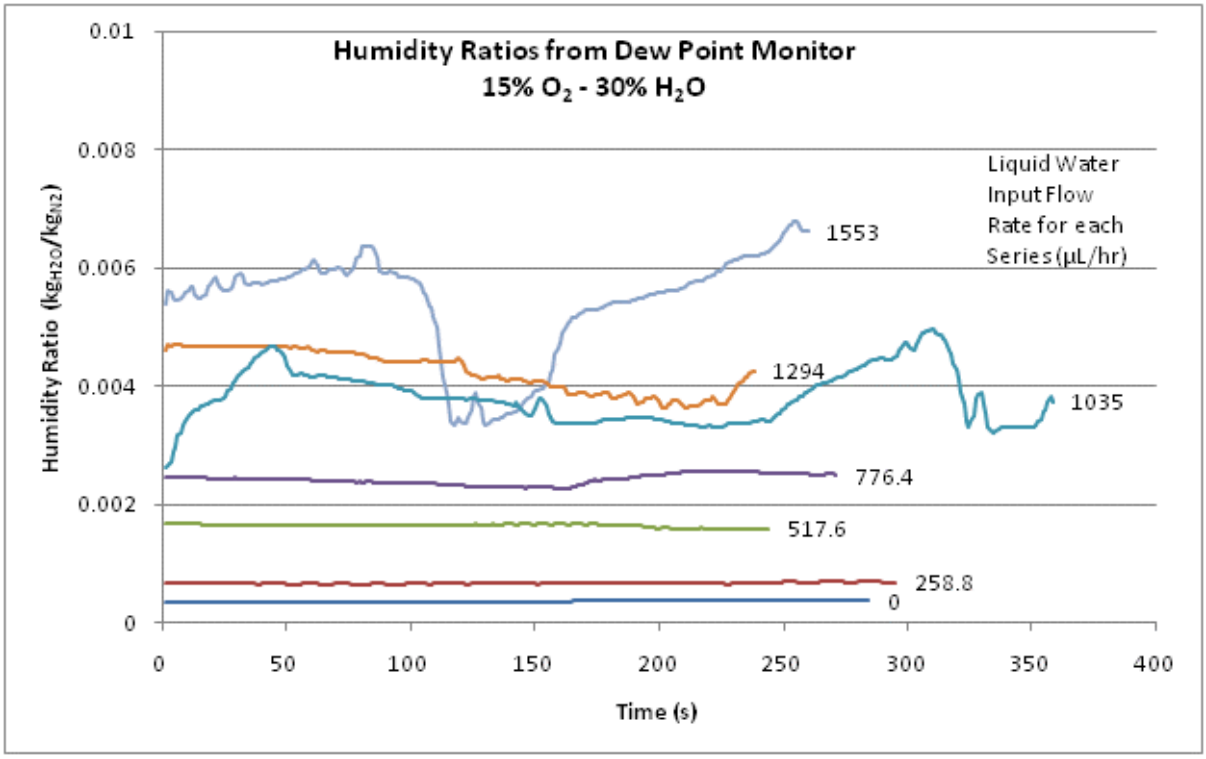


**Figure 2-6: Example of output humidity ratio data from dew point monitor.**

Once the steady addition of water vapor into the gas stream was confirmed, the experimental apparatus was adjusted to take ignition temperature data. Figure 2-7 diagrams this setup. All three gases were metered individually through Porter mass flow controllers. Each flow was again controlled then confirmed with the NI-9263 CompacDAQ and the Omega DAQ-56, respectively. The propane and nitrogen streams combined before the water addition at the heating coil and the oxygen was introduced at the mixing nozzle. The homogenous mixture exited the nozzle as a steady stream at constant velocity and traveled through the quartz tube and over the platinum coil. The wire was electrically heated by a Keithley® 2440 SourceMeter. The SourceMeter was purchased to replace the power supply as well as the digital multimeter used by Lounsbury [3]. The SourceMeter operates in a constant current mode, or sweeps through a specified range of currents, while simultaneously taking a four-point measurement of the resistance of the platinum wire catalyst. This greatly improves the accuracy of the measurements due to the elimination of manually setting the current and recording the resistance. Using the SourceMeter, the source current is accurate to ± (0.1% + 3.42 mA) up to the 5 A maximum source current and the resistance measurement is accurate to ± (0.17% + 0.0003 Ω). The previously used power supply had a constant current operating range of 0 to 60 A and was accurate to ± (0.1% + 40 mA). For this research, the maximum amperage input was 1.7 A, so the previous maximum input error was 41.7 mA, whereas using the SourceMeter, the new maximum error was only 5.12 mA. The experimental uncertainty due to the SourceMeter accuracy is given in Table 2.1 and shown in Figure 2-8 with the power input vs. temperature curve for air flow over the wire.

**Table 2.1: Experimental Uncertainty due to SourceMeter Accuracy**

| P (W) | Uncertainty (W) | $T_{ave}$ (K) | Uncertainty (K) |
|---|---|---|---|
| 1.0 | $\pm$ 0.0109 | 361.2 | $\pm$ 0.609 |
| 2.0 | $\pm$ 0.0178 | 421.3 | $\pm$ 0.711 |
| 3.0 | $\pm$ 0.0242 | 478.3 | $\pm$ 0.808 |
| 4.0 | $\pm$ 0.0304 | 532.0 | $\pm$ 0.899 |
| 5.0 | $\pm$ 0.0364 | 582.4 | $\pm$ 0.985 |
| 6.0 | $\pm$ 0.0422 | 629.7 | $\pm$ 1.065 |
| 7.0 | $\pm$ 0.0480 | 673.7 | $\pm$ 1.140 |
| 8.0 | $\pm$ 0.0536 | 714.5 | $\pm$ 1.209 |
| 9.0 | $\pm$ 0.0590 | 752.0 | $\pm$ 1.273 |

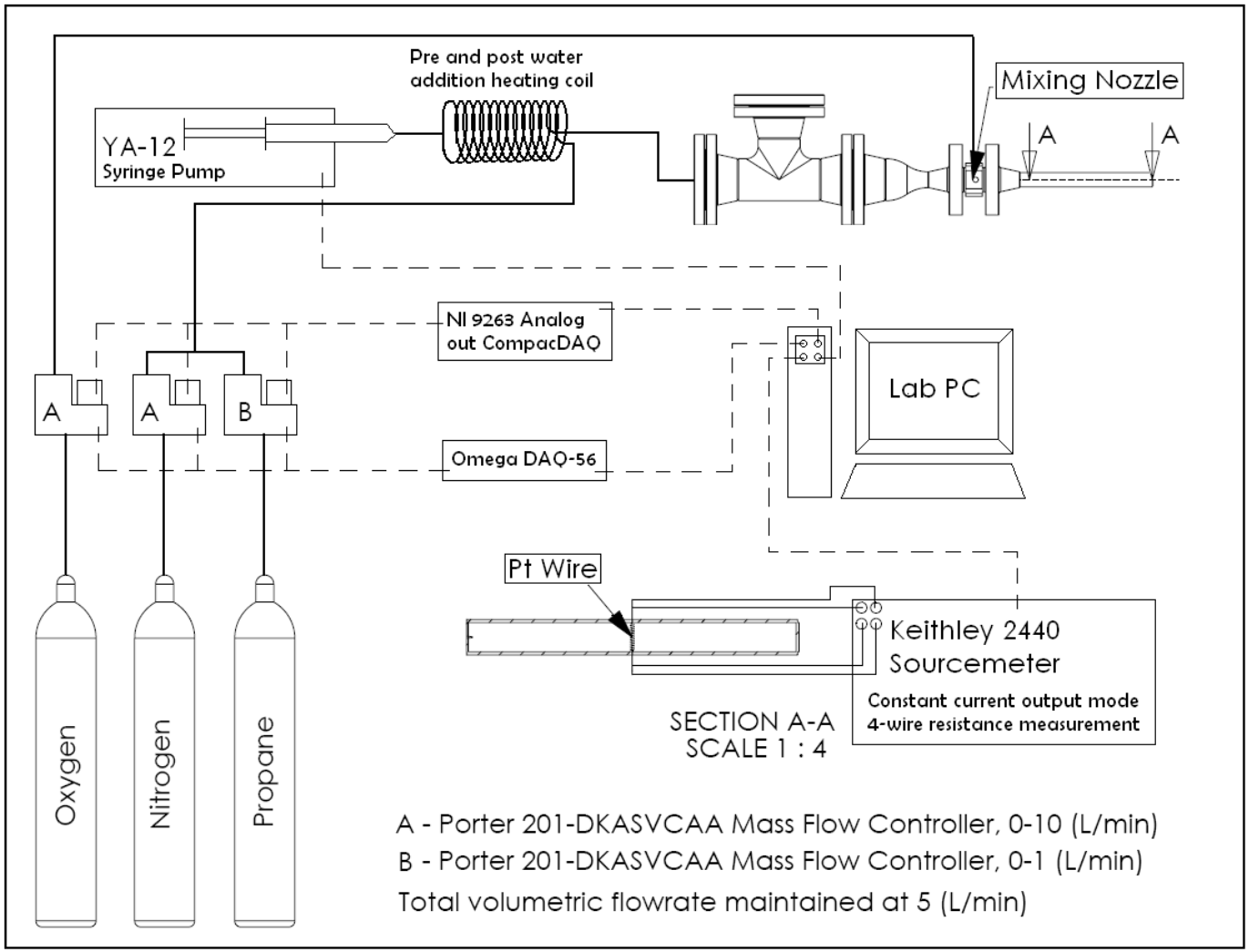


**Figure 2-7: Experimental schematic for ignition temperature data collection.**

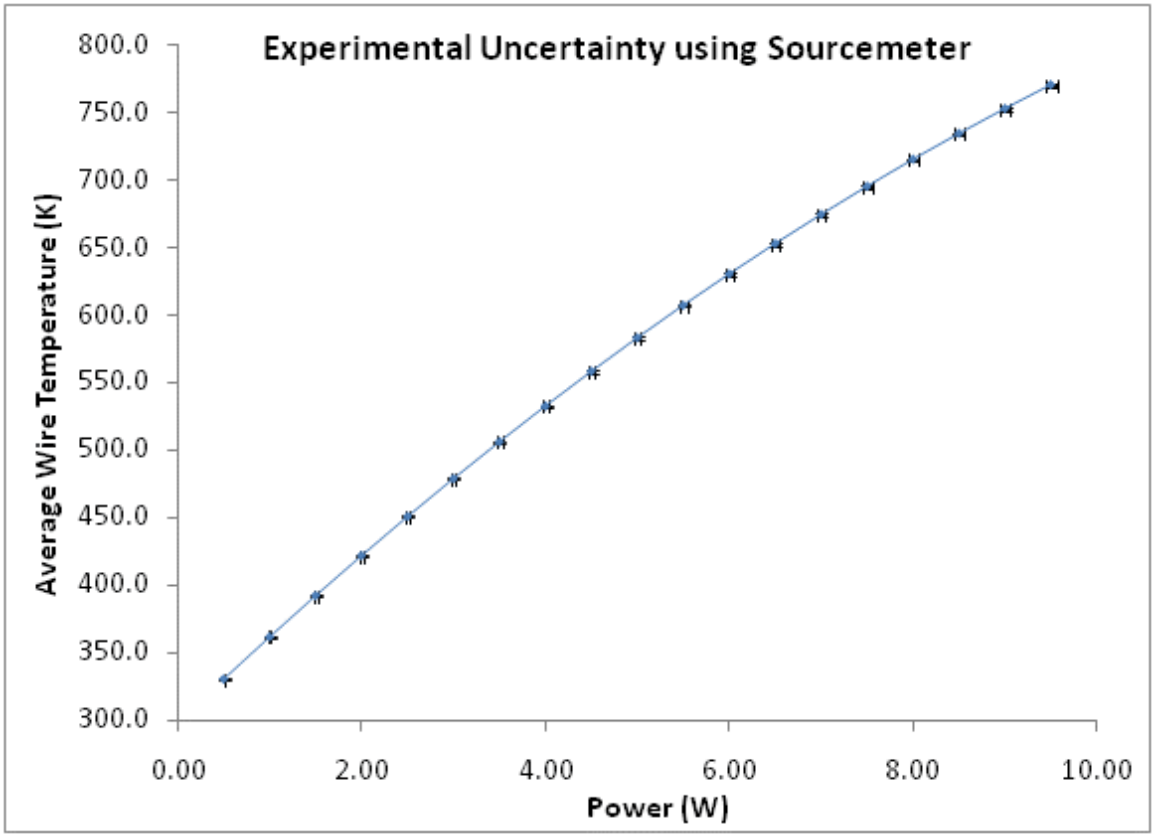


**Figure 2-8: T vs. power curve for air flow over the wire with experimental uncertainty.**

## 2.2 Methods

As explained in [3], the platinum wire acts as a microcalorimeter, monitoring small changes in heat flow due to voltage fluctuations. By simply measuring the electrical resistance of the wire, the ignition temperature, power at ignition, and heat generation from surface reactions could be determined.

With known current and resistance values, the power input to the wire was found using Equation 2.1.

$$P = I^2 R \qquad \textbf{Equation 2.1}$$

**Equation 2.2**

$$R = R_0[1 + \alpha(T - T_0)]$$

From Equation 2.2, the temperature of the wire was found by the linear correlation between resistance and temperature [16, p 245] where, $R_0$ is the resistance at $T_0$, and α is the temperature coefficient of resistance, with α=0.003927 for platinum. For the 127 μm diameter wire with a length of 0.14224 m that was used throughout this study, $R_0$=1.276 Ω at $T_0$=293 K. This measurement was taken using the SourceMeter with an input current, I=0.001A. These parameters were entered into LabView®, where power and temperature could be directly calculated once the resistance measurements were taken.

Resistance measurements were first taken with 5 $^{L}/_{min}$ of air flowing over the wire. The SourceMeter was set to sweep through a range of currents, from 0.1 A to 1.7 A, while recording the wire resistance, taking 1500 $^{readings}/_{Amp}$ at about 14 $^{readings}/_{sec}$. These rates were confirmed to give accurate results by manually setting a constant current and recording the resistance after it reached steady state for multiple current values. An example of results from this constant current method is shown in Figure 2-10. Both methods gave equivalent power vs. temperature curves, verifying the current sweep method, which was used for the rest of the experiments. However, for the reactive mixtures, the maximum current was set between 1.2 and 1.45, depending on the propane content, to avoid melting through the wire.

When the wire was exposed to reactive mixtures, as the power increased, the propane began reacting on the platinum surface, causing a jump in temperature and power and marking the ignition point. The LabView® algorithm for finding this point, as well as the power generated from surface reactions, is depicted in Figure 2-9. First, LabView® calculates a line using the steepest slope of the temperature increase with power, Line A in Figure 2-9. Line A represents the ramp-up curve between when reactions initiate and where they reach a constant rate. Where this line crosses the air curve is considered the ignition point, Point 1. The power and temperature at this point are what will be referred to as the "ignition power" and the "ignition temperature," or $P_{ign}$ and $T_{ign}$ respectively.

To find the energy generation, $Q_{gen}$, from surface reactions, we need to find the point that the power and temperature increase once reactions begin. This is labeled as Point 2 in Figure 2-9. LabView® adds an offset to the air curve that gives Line B, the new wire temperature once constant reactions occur. Where Line A and Line B intersect gives Point 2. So, Point 1 represents the initiation of surface reactions, causing an increase in power and temperature up to Point 2. If the wire were to be maintained at this new temperature in air, the power necessary corresponds to Point 3. Therefore, the difference in power between Points 3 and 1 is considered to be the power generated from surface reactions on the catalyst. Figure 2-9 shows this entire process and equivalence ratio of $\varphi$=0.8 at 12.5% cxygen by volume. The process is identical for any reactive mixture.

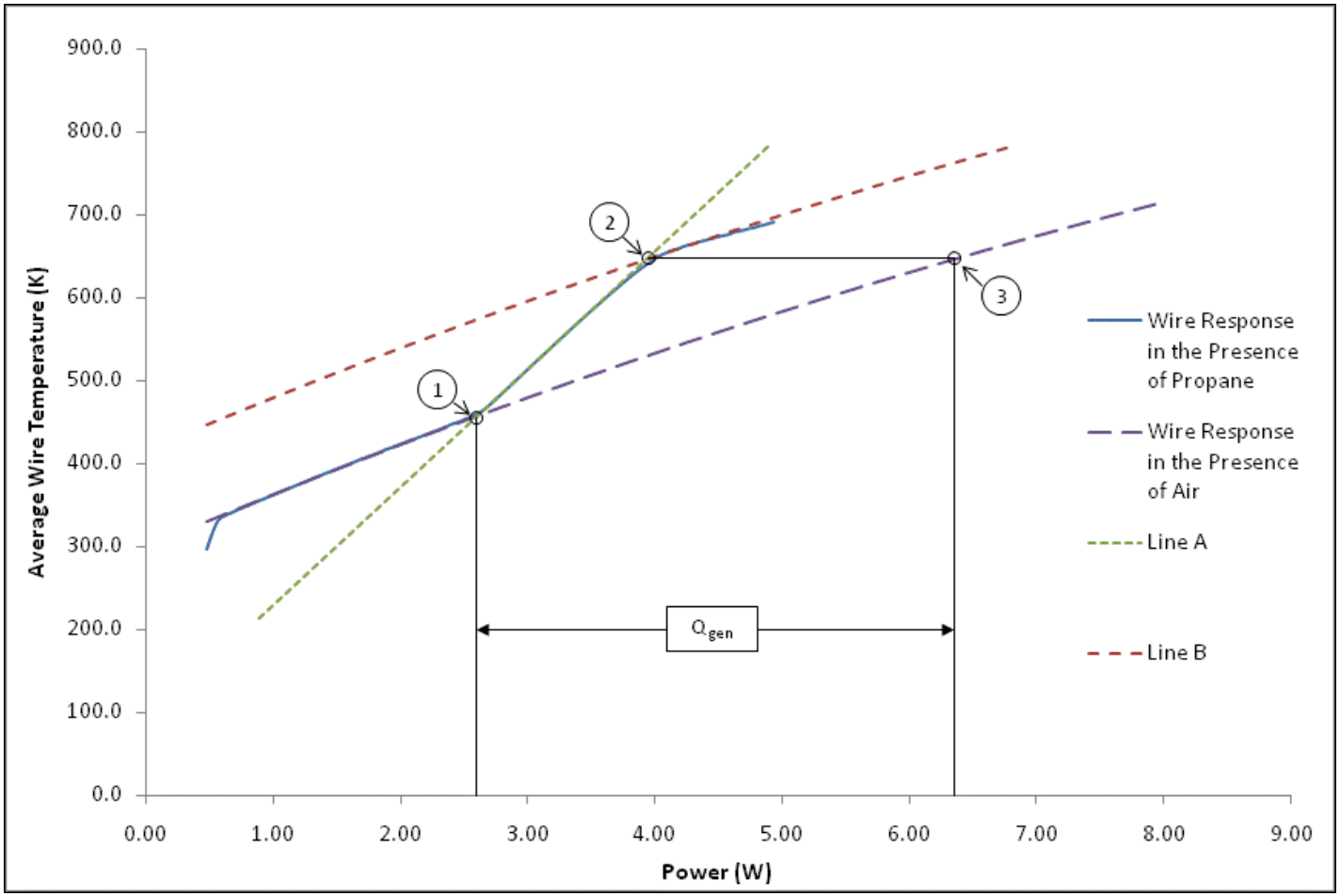


**Figure 2-9: Calculating $Q_{gen}$, the heat generation from reactions on the catalyst surface.**

Figure 2-10 shows an example SourceMeter output for a constant current input rather than a current sweep. The average wire temperature and power input as a function of time was calculated from the same mixture used in Figure 2-9 above, 12.5% fixed volume oxygen and $\varphi$=0.8. It can be seen that either the constant current or the sweep method gave the same result. In this case, a temperature jump from approximately 450 K to 650 K and a power jump from around 2.7 W to 4 W. However, without using the sweep method, the constant current had to be entered multiple times until a power just below the ignition power was reached and gradually increased up to the ignition point. The current sweep method proved to be much more efficient for data collection because the SourceMeter was gradually increasing the current at a constant rate instead of adjusting it manually. The jump in power and temperature was still seen once the ignition point was reached. However, since the current was continually increased, once the reactions had reached steady-state, the power and temperature continued to rise, shown by Line B in Figure 2-9. The constant current method was useful in finding the time response of the system, and it was found that about 4 seconds after ignition the reaction rate reached steady-state.

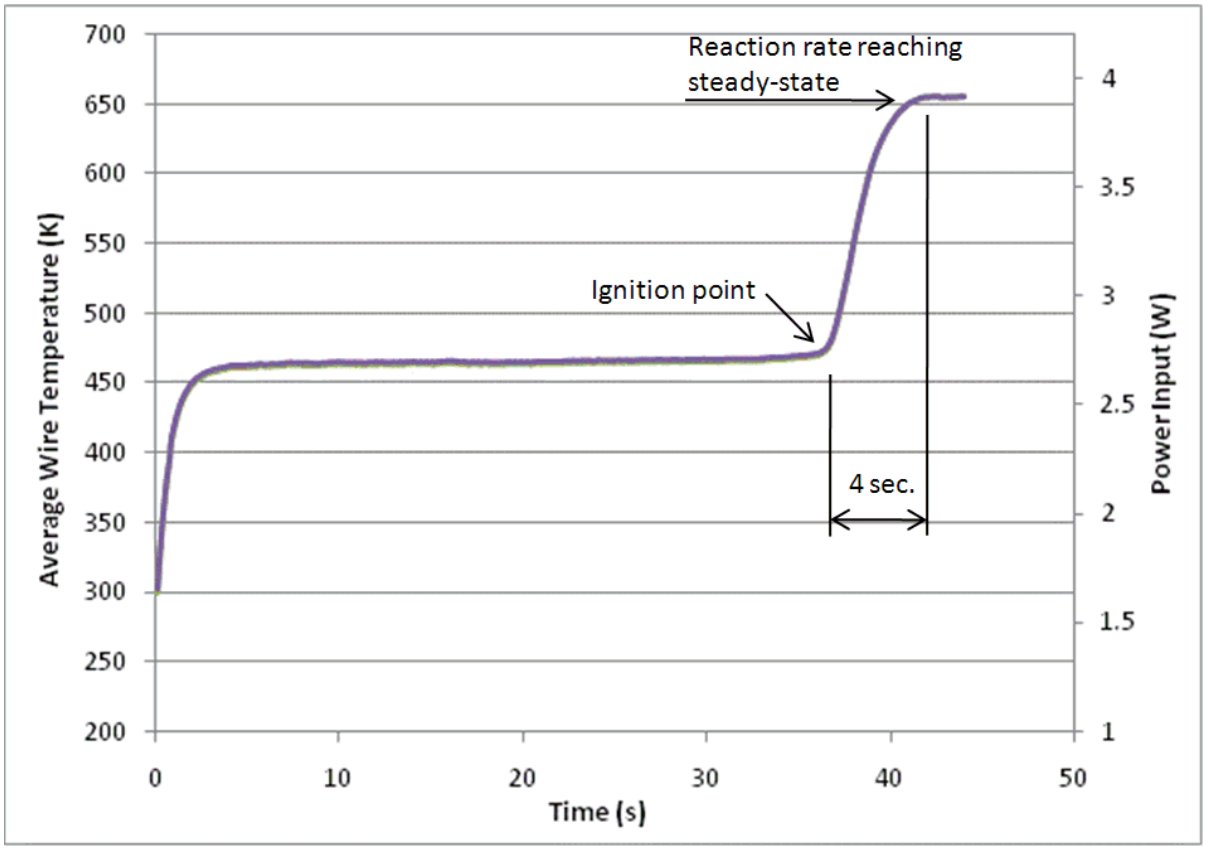


**Figure 2-10: T and power input vs. time with a constant current input.**

# 3 Experimental Results

The propane-oxygen and propane-oxygen-water mixtures were run with a total volume flow rate of 5 $^{L}/_{min}$ over a 127 μm diameter coiled platinum wire catalyst. Average wire temperature data was first collected with 5 $^{L}/_{min}$ of air flowing over the catalyst as the power input to the wire was increased. This gave a baseline for the experiments with reactive mixtures and was also necessary to carry out the calculations described in Section 2.2.

## 3.1 Average Wire Temperature vs. Power

For the reactive mixtures, experiments were run with either fixed volumes of propane or with fixed volumes of oxygen. At each fixed volume, experiments were run dry and with 10%, 20%, 30% and 40% water vapor to propane ratio by volume ($w_r$). For each of these sets, experiments were run through equivalence ratios of $0.1 \leq \varphi \leq 1.0$ unless they fell within the flammable range or were too far beyond the range of steady state water vapor addition. The experiment matrix is shown in Table 3.1 and the results are in the following figures. The tables within these figures contain the $T_{ign}$ (K) and $Q_{gen}$ (W) values calculated in LabView® using the method described in Section 2.2 and Figure 2-9. For brevity, only representative samples of the temperature/power plots are included here (see Leichliter [29] for details). To convert $Q_{gen}$ to flux, divide by the nominal surface area of the wire exposed to reacting flow (0.608 $cm^2$).

**Table 3.1: Experiment Matrix**

| | Dry | $w_r$ = 10% | $w_r$ = 20% | $w_r$ = 30% | $w_r$ = 40% |
|---|---|---|---|---|---|
| **1.0% Propane** | $0.3 \leq \varphi \leq 1.0$ | $0.3 \leq \varphi \leq 1.0$ | $0.3 \leq \varphi \leq 1.0$ | $0.3 \leq \varphi \leq 1.0$ | $0.3 \leq \varphi \leq 1.0$ |
| **1.5% Propane** | $0.4 \leq \varphi \leq 1.0$ | $0.4 \leq \varphi \leq 1.0$ | $0.4 \leq \varphi \leq 1.0$ | $0.4 \leq \varphi \leq 1.0$ | - |
| **2.0% Propane** | $0.5 \leq \varphi \leq 1.0$ | $0.5 \leq \varphi \leq 1.0$ | $0.5 \leq \varphi \leq 1.0$ | - | - |
| **5.0% Oxygen** | $0.1 \leq \varphi \leq 1.0$ | $0.3 \leq \varphi \leq 1.0$ | $0.5 \leq \varphi \leq 1.0$ | $0.1 \leq \varphi \leq 1.0$ | $0.1 \leq \varphi \leq 1.0$ |
| **7.5% Oxygen** | $0.1 \leq \varphi \leq 1.0$ | $0.2 \leq \varphi \leq 1.0$ | $0.4 \leq \varphi \leq 1.0$ | $0.1 \leq \varphi \leq 1.0$ | $0.1 \leq \varphi \leq 1.0$ |
| **10.0% Oxygen** | $0.1 \leq \varphi \leq 1.0$ | $0.3 \leq \varphi \leq 1.0$ | $0.2 \leq \varphi \leq 1.0$ | $0.1 \leq \varphi \leq 1.0$ | $0.1 \leq \varphi \leq 0.7$ |
| **12.5% Oxygen** | $0.1 \leq \varphi \leq 0.8$ | $0.3 \leq \varphi \leq 0.8$ | $0.1 \leq \varphi \leq 0.8$ | $0.1 \leq \varphi \leq 0.8$ | $0.1 \leq \varphi \leq 0.8$ |
| **15.0% Oxygen** | $0.1 \leq \varphi \leq 0.6$ | $0.2 \leq \varphi \leq 0.6$ | $0.1 \leq \varphi \leq 0.6$ | $0.1 \leq \varphi \leq 0.6$ | $0.1 \leq \varphi \leq 0.6$ |
| **17.5% Oxygen** | $0.1 \leq \varphi \leq 0.5$ | $0.2 \leq \varphi \leq 0.5$ | $0.1 \leq \varphi \leq 0.5$ | $0.1 \leq \varphi \leq 0.5$ | $0.1 \leq \varphi \leq 0.4$ |
| **20.0% Oxygen** | $0.1 \leq \varphi \leq 0.5$ | $0.2 \leq \varphi \leq 0.5$ | $0.1 \leq \varphi \leq 0.5$ | $0.1 \leq \varphi \leq 0.4$ | $0.1 \leq \varphi \leq 0.2$ |

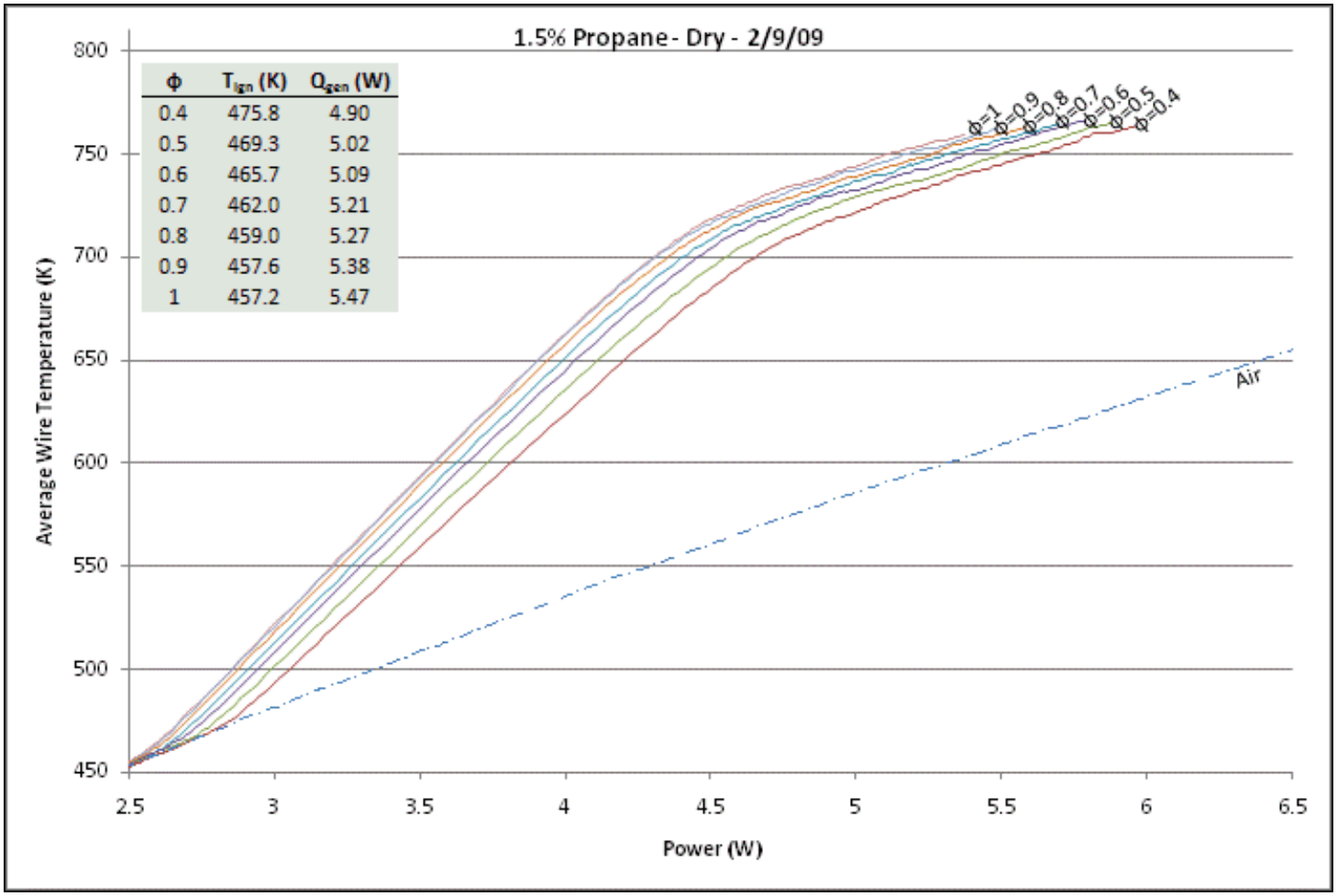


| ϕ | $T_{ign}$ (K) | $Q_{gen}$ (W) |
|---|---|---|
| 0.4 | 475.8 | 4.90 |
| 0.5 | 469.3 | 5.02 |
| 0.6 | 465.7 | 5.09 |
| 0.7 | 462.0 | 5.21 |
| 0.8 | 459.0 | 5.27 |
| 0.9 | 457.6 | 5.38 |
| 1 | 457.2 | 5.47 |

**Figure 3-1: Average wire temperature vs. power for 1.5% fixed propane, dry.**

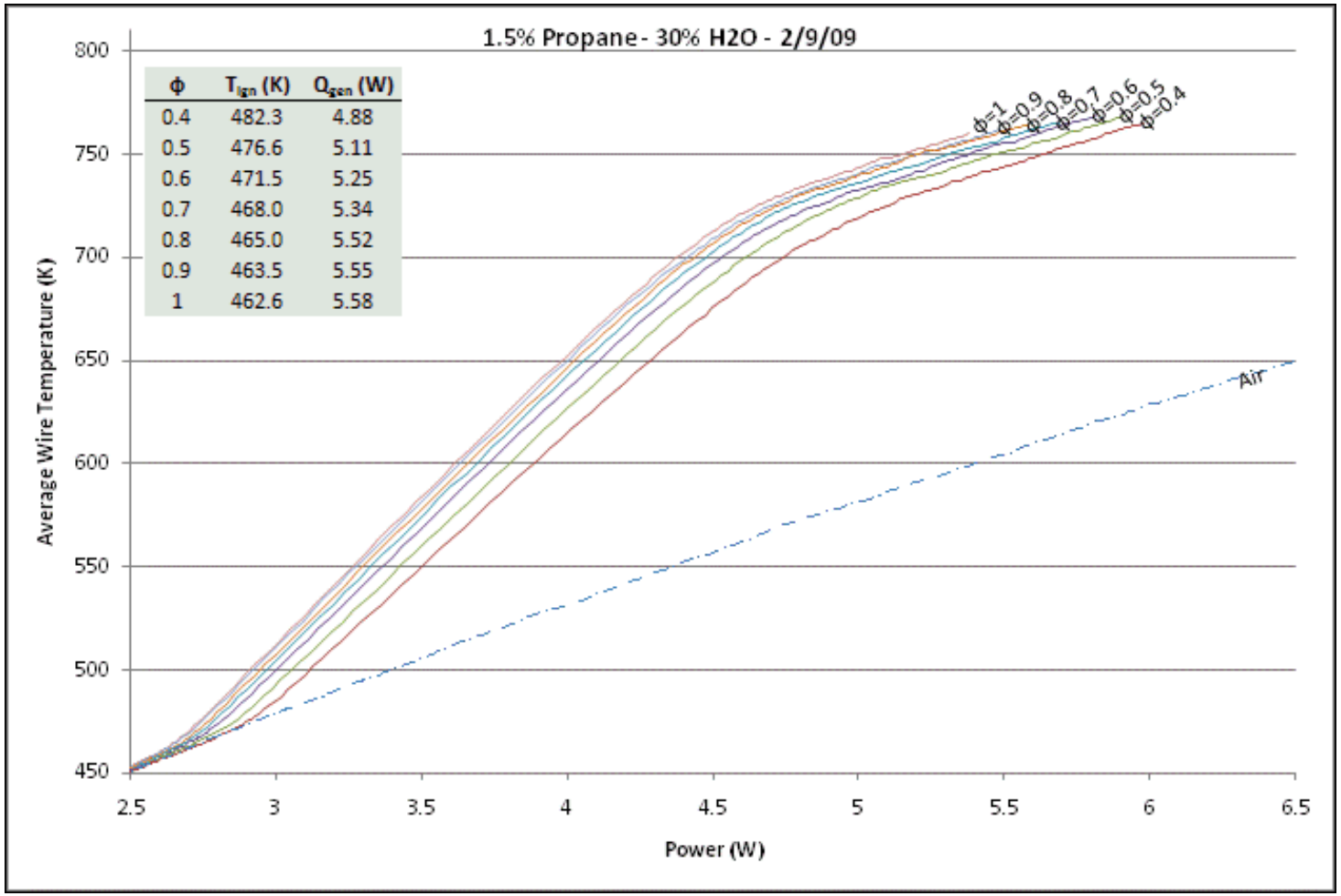


| ϕ | $T_{ign}$ (K) | $Q_{gen}$ (W) |
|---|---|---|
| 0.4 | 482.3 | 4.88 |
| 0.5 | 476.6 | 5.11 |
| 0.6 | 471.5 | 5.25 |
| 0.7 | 468.0 | 5.34 |
| 0.8 | 465.0 | 5.52 |
| 0.9 | 463.5 | 5.55 |
| 1 | 462.6 | 5.58 |

**Figure 3-2: Average wire temperature vs. power for 1.5% fixed propane, 30% water.**

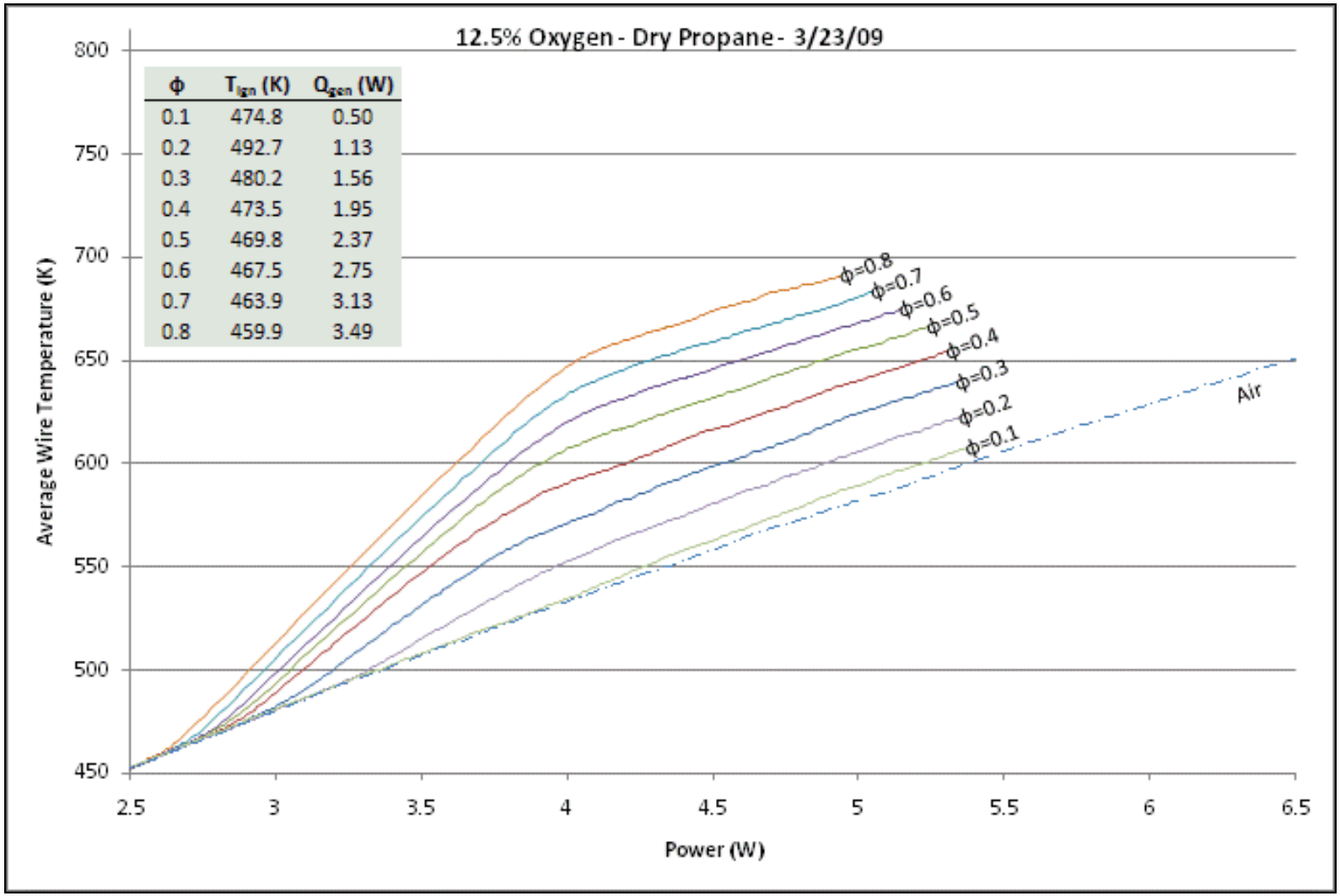


| ϕ | $T_{ign}$ (K) | $Q_{gen}$ (W) |
|---|---|---|
| 0.1 | 474.8 | 0.50 |
| 0.2 | 492.7 | 1.13 |
| 0.3 | 480.2 | 1.56 |
| 0.4 | 473.5 | 1.95 |
| 0.5 | 469.8 | 2.37 |
| 0.6 | 467.5 | 2.75 |
| 0.7 | 463.9 | 3.13 |
| 0.8 | 459.9 | 3.49 |

**Figure 3-3: Average wire temperature vs. power for 12.5% fixed oxygen, dry.**

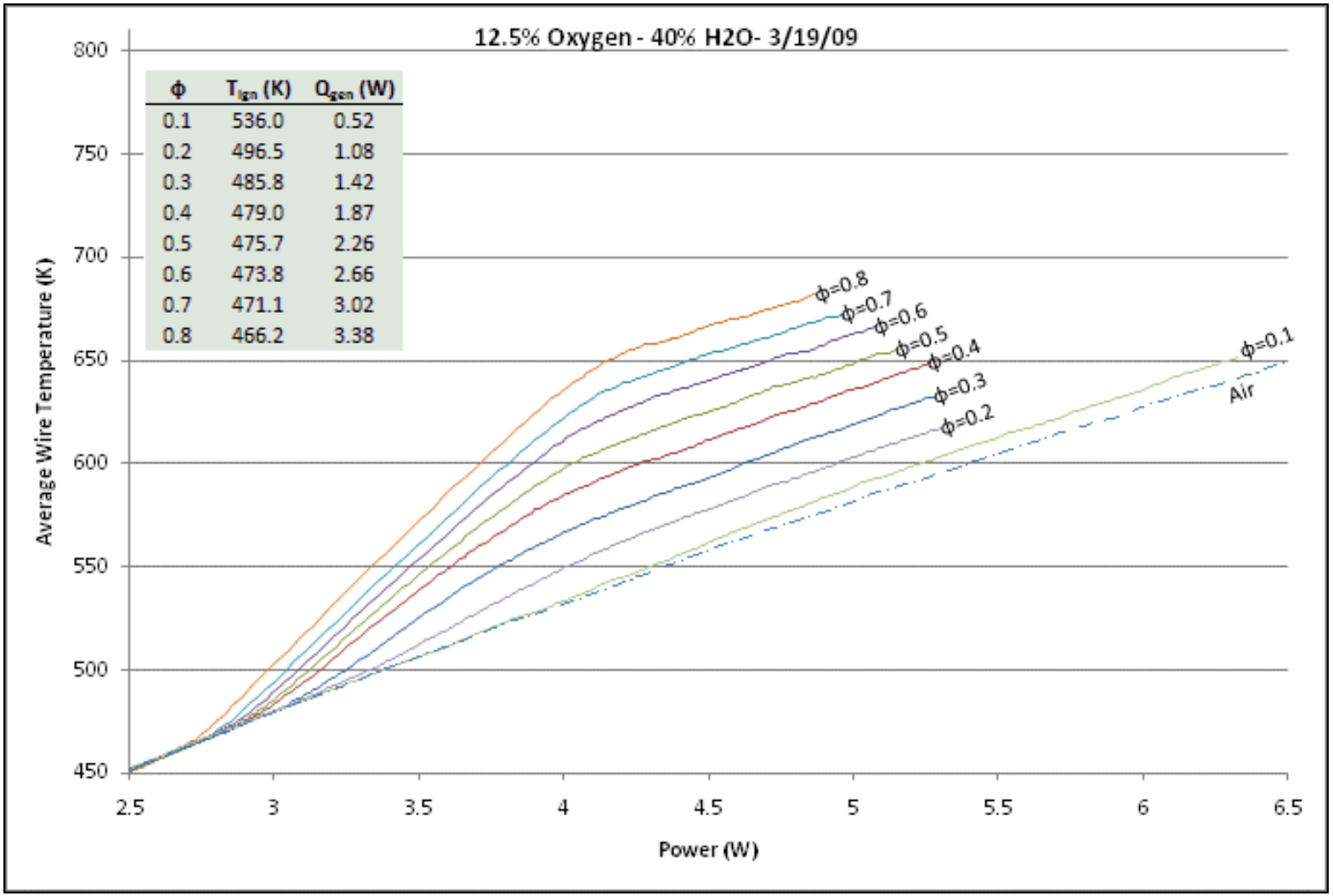


| ϕ | $T_{ign}$ (K) | $Q_{gen}$ (W) |
|---|---|---|
| 0.1 | 536.0 | 0.52 |
| 0.2 | 496.5 | 1.08 |
| 0.3 | 485.8 | 1.42 |
| 0.4 | 479.0 | 1.87 |
| 0.5 | 475.7 | 2.26 |
| 0.6 | 473.8 | 2.66 |
| 0.7 | 471.1 | 3.02 |
| 0.8 | 466.2 | 3.38 |

**Figure 3-4: Average wire temperature vs. power for 12.5% fixed oxygen, 40% water.**

A major observation seen from these results and discussed in previous work [3] was the difference in behavior of a “seasoned” wire compared to a “fresh” wire. A seasoned wire refers to a wire that has been exposed to surface reactions, where a fresh wire has not. Figure 3-5 was taken from [3] and shows the reactivity on the surface increases significantly after the initial exposure to surface reactions. Not only is the energy generation due to surface reactions much greater when using a seasoned wire over a fresh one, but less power input is necessary for the reactions to initiate. However, in this study, a continuation of the seasoning phenomena was seen where after the initial decrease in ignition temperature and increase in $Q_{gen}$, the wire continues to change causing a gradual increase in $T_{ign}$ and a decrease in $Q_{gen}$. This can be seen in Figure 3-6, where neither of the curves are from a “fresh” wire. However, there is still a distinct change in the behavior of the wire. This behavior change is likely due to pitting and erosion or impurities on the wire surface, changing the surface site density for reactions to take place (Figure 3-7 and Figure 3-8). This change in wire behavior over time is important to the design of the CPT igniter because as the reactivity of the platinum decreases, the ignition timing is affected.

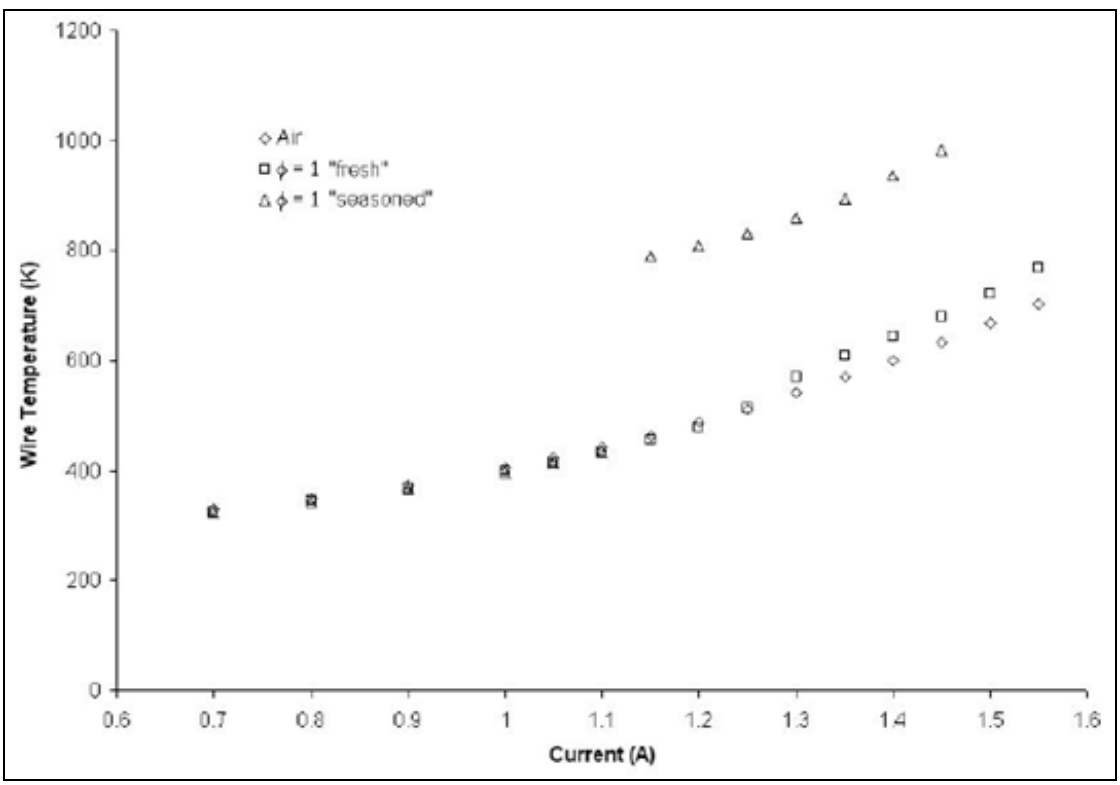


**Figure 3-5: Wire temperature vs. current for a 'seasoned' wire compared to a 'fresh' wire [3].**

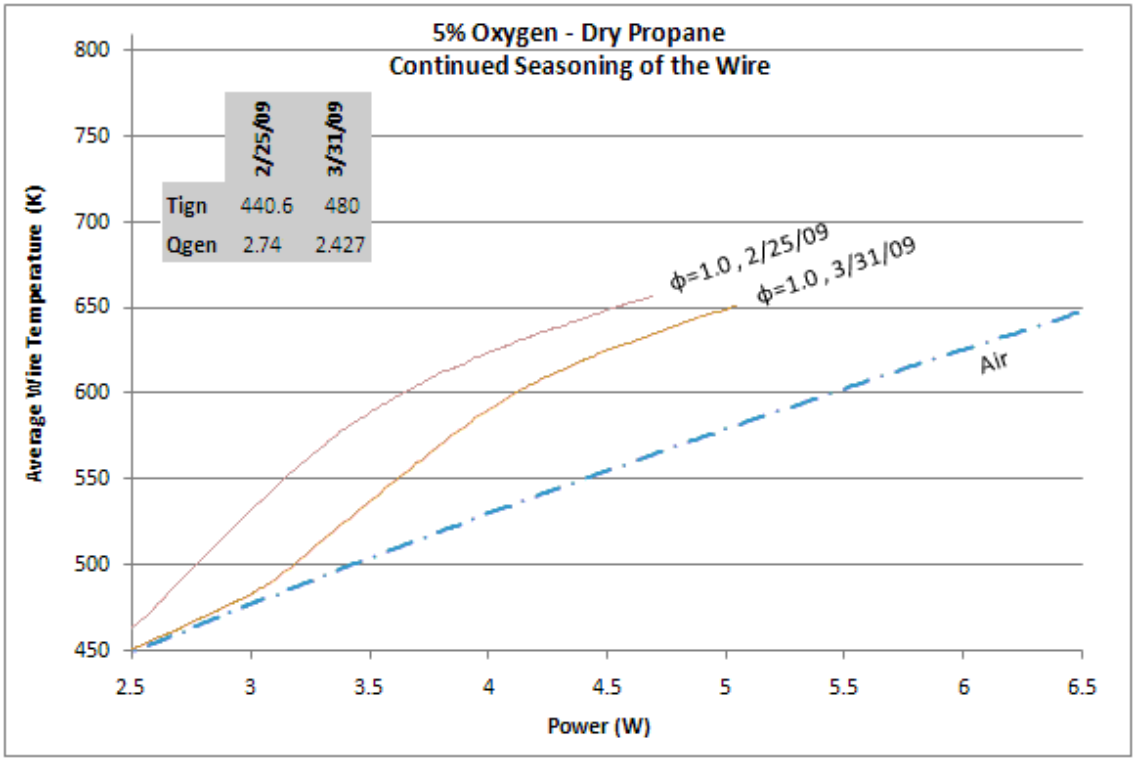


**Figure 3-6: Temperature vs. Power for 5% $O_2$ on two different dates.**

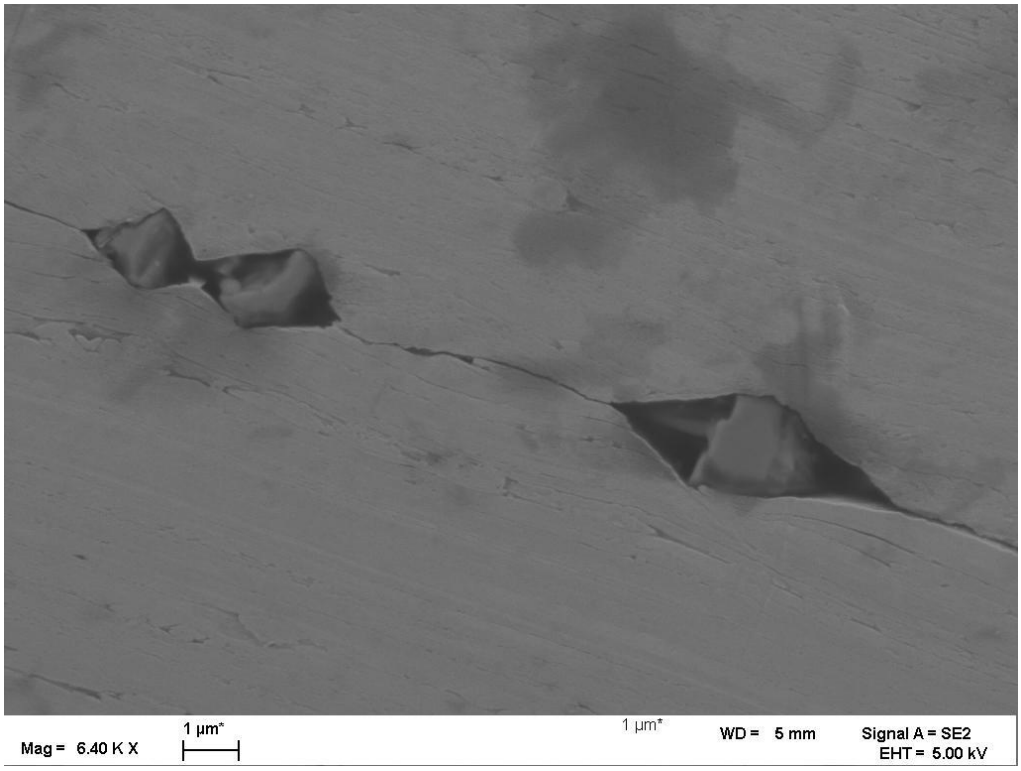


**Figure 3-7: Unseasoned Pt wire showing small grain boundaries and inclusions.**


**Figure 3-8: Seasoned Pt wire with grain boundary growth and deposits on reaction sites.**

## 3.2 Ignition Temperature and Surface Reaction Energy Generation Calculations

Once all the data was collected, the ignition temperatures were plotted as a function of the mass fraction of oxygen or fuel as shown in Figure 3-7 and Figure 3-8. Since all mixtures were considered to be ideal gases throughout this study, the mass fraction of any component is equivalent to the volume fraction or fixed volume percentage of that same component. The expected trends can be seen more clearly in Figure 3-7, depicting the fixed propane results, than in Figure 3-8 the plot of fixed oxygen results. This may be due to the timing or order in which the experiments were run and will be discussed further later in this section. However, from the fixed propane results shown in Figure 3-7, it is evident that as the percentage of propane increases, or the percentage of oxygen decreases, the ignition temperature and consequently ignition power decrease. Therefore, mixtures with higher fuel to oxygen ratios,

$x_F/x_{O_2}$, require less power input to initiate the surface reactions, which is expected for these fuel-lean mixtures.

The results for the energy generated from surface reactions for the dry experiments are shown in Figure 3-9 and Figure 3-10 for fixed propane and fixed oxygen, respectively. Again, the trends are more evident from the fixed propane data, showing more energy generated from the surface reactions for mixtures with higher propane and lower oxygen content.

A comparison of calculated ignition temperatures with that of Lounsbury [3] and Cho and Law [2] is shown in Figure 3-11. The difference between the ignition temperatures from Cho and Law [2] and those calculated by Lounsbury [3] where attributed to use of only “fresh” wires by Cho and Law [2] and continuous use of a “seasoned” wires by Lounsbury in [3]. The discrepancies between the experimental ignition temperatures found in this study and those calculated by Lounsbury [3] are likely due to the continuing seasoning effect described above and displayed in Figure 3-6. Figure 3-11also displays the φ=0.1 data not following the expected trend, also discussed above.

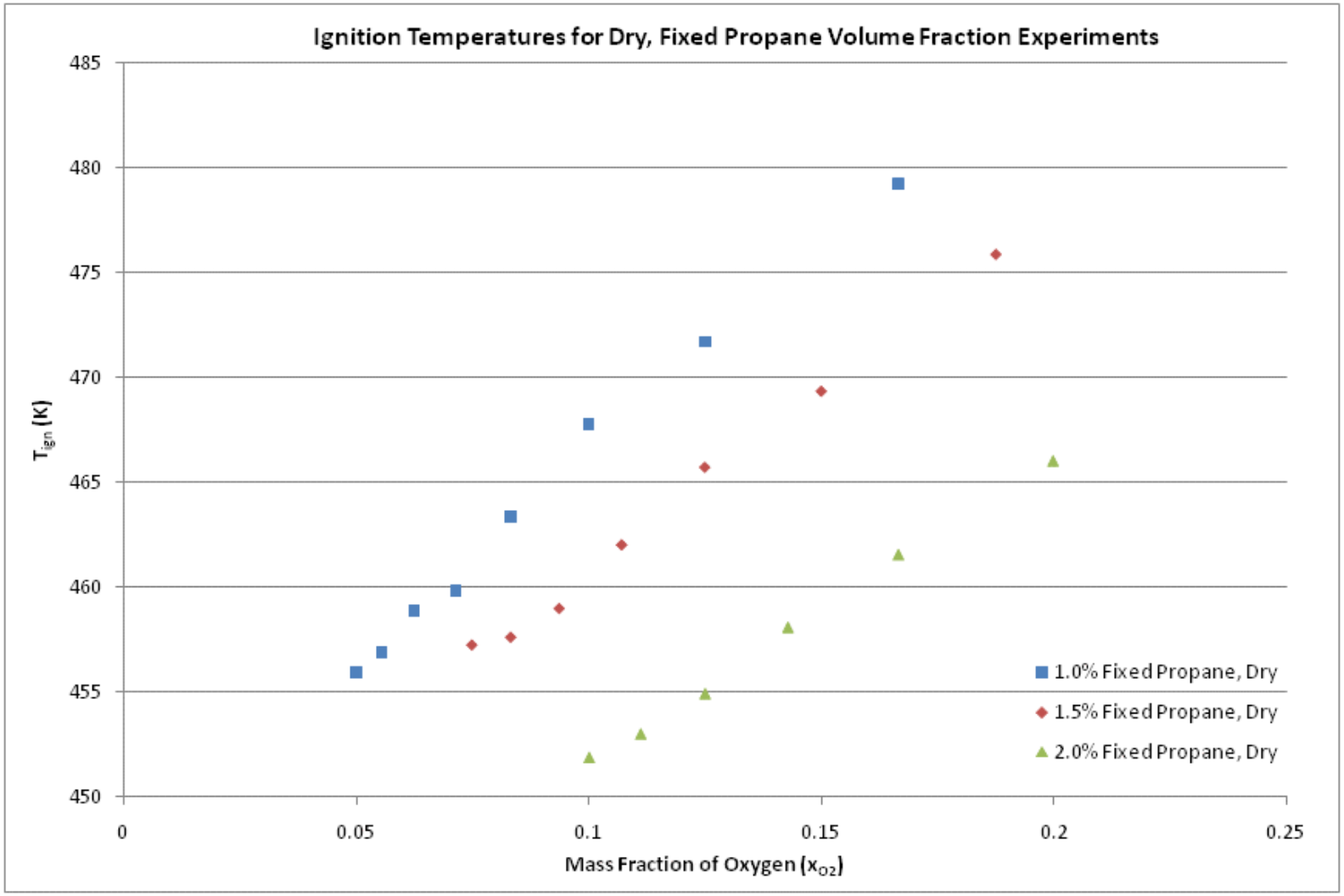


**Figure 3-9: Summary of ignition temperatures for fixed volume dry propane mixtures.**

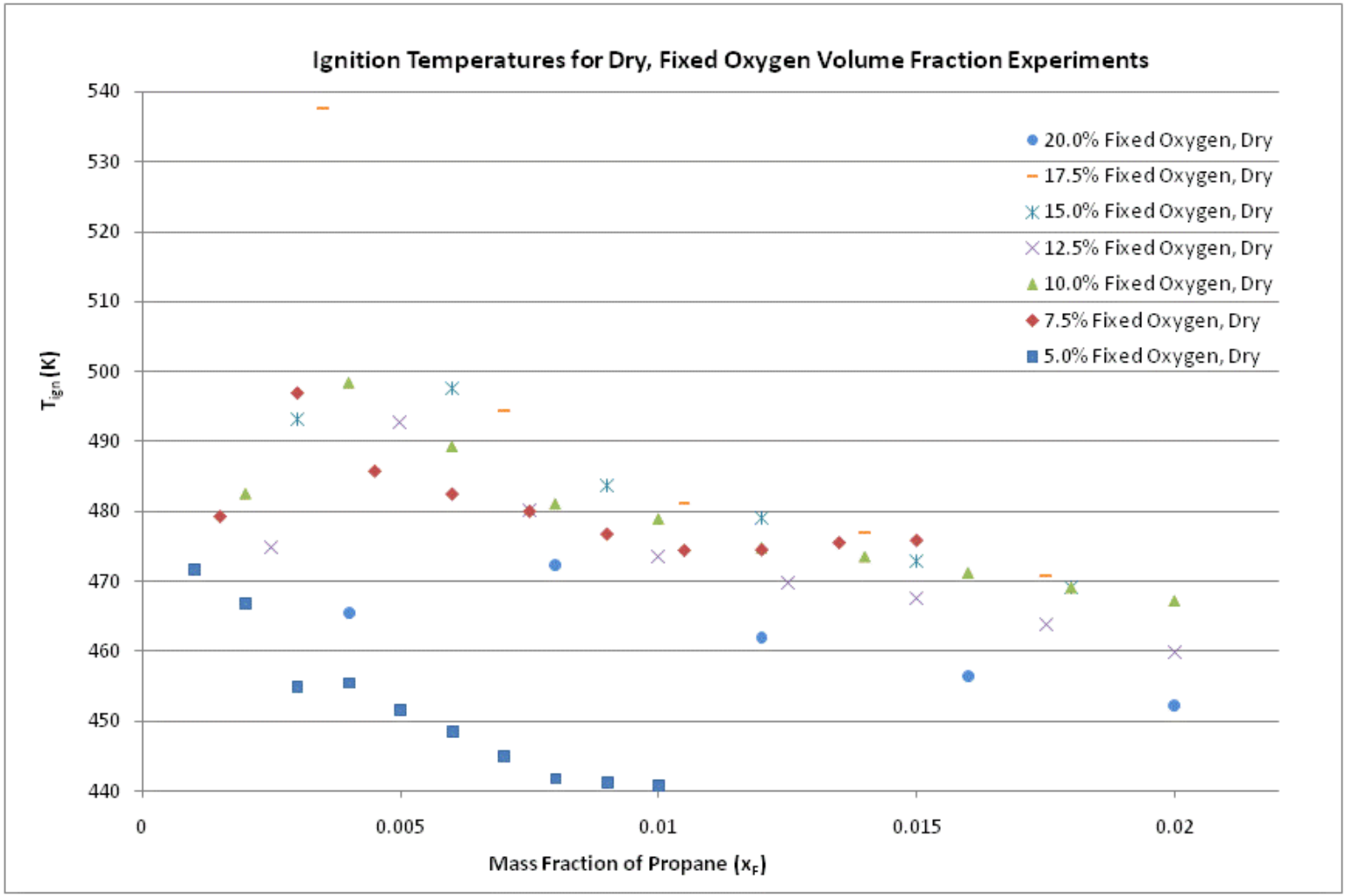


**Figure 3-10: Summary of ignition temperatures for fixed volume dry oxygen mixtures.**

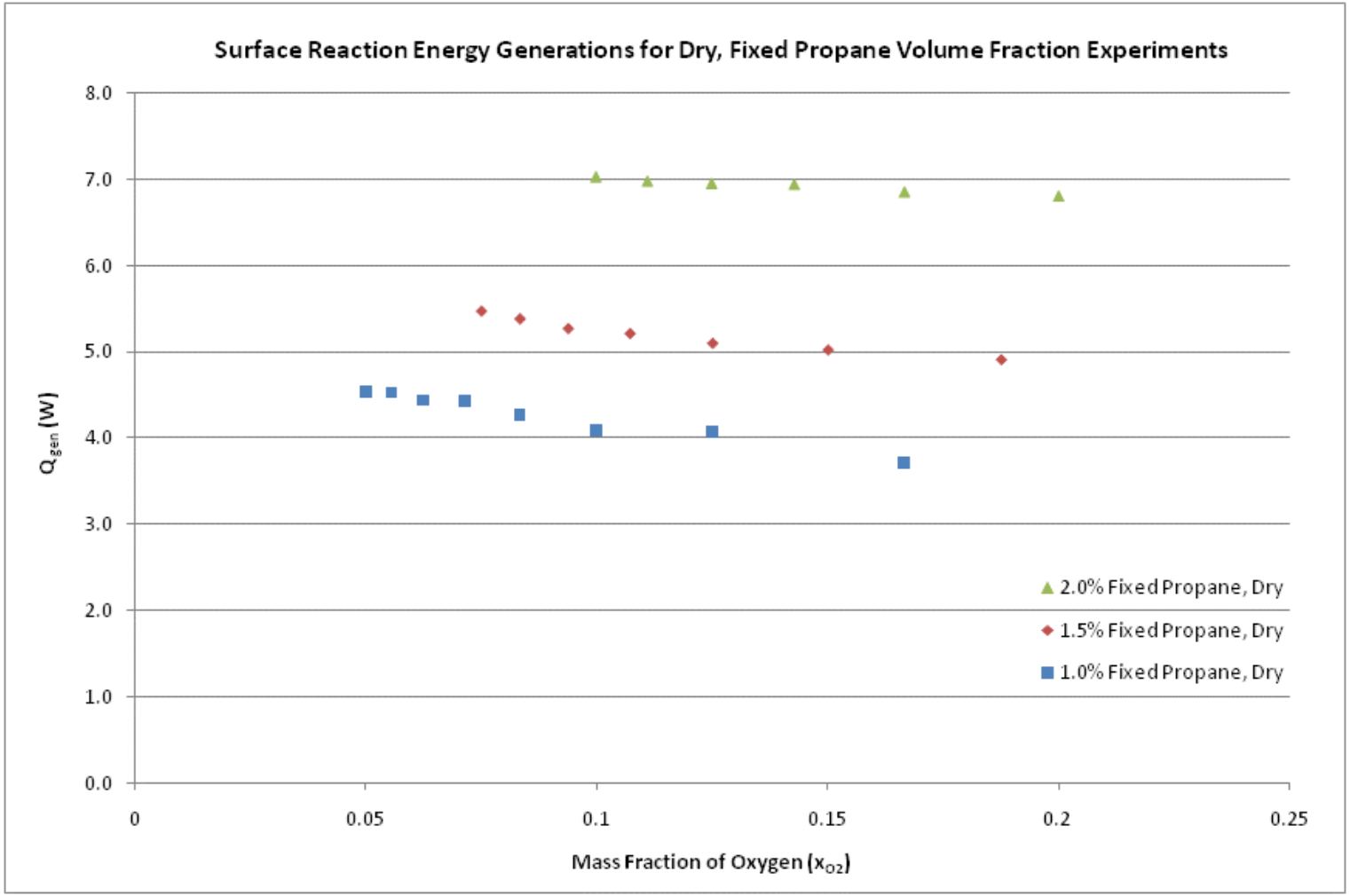


**Figure 3-11: Summary of $Q_{gen}$ for fixed volume dry propane mixtures.**

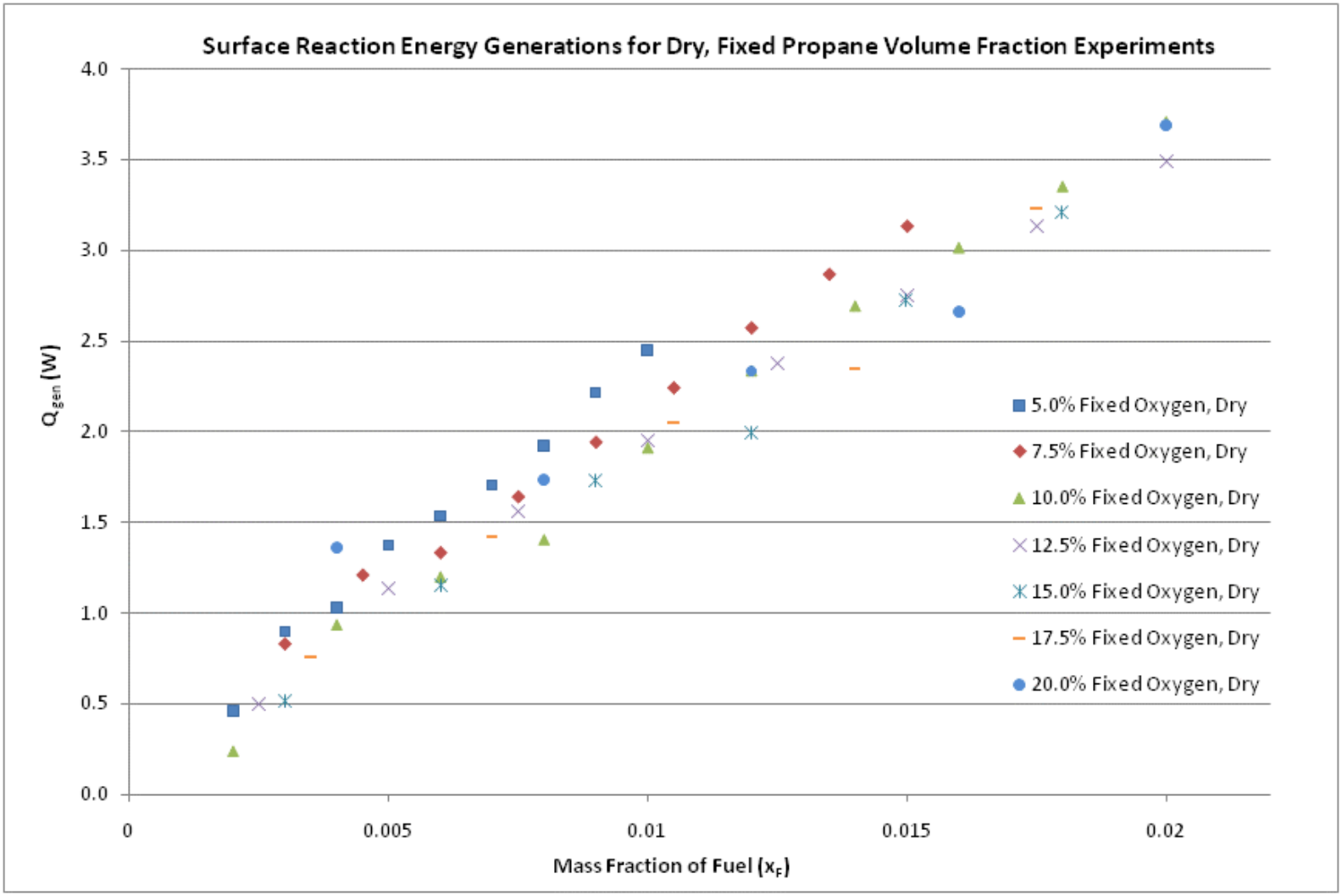


**Figure 3-12: Summary of $Q_{gen}$ for fixed volume dry oxygen mixtures.**

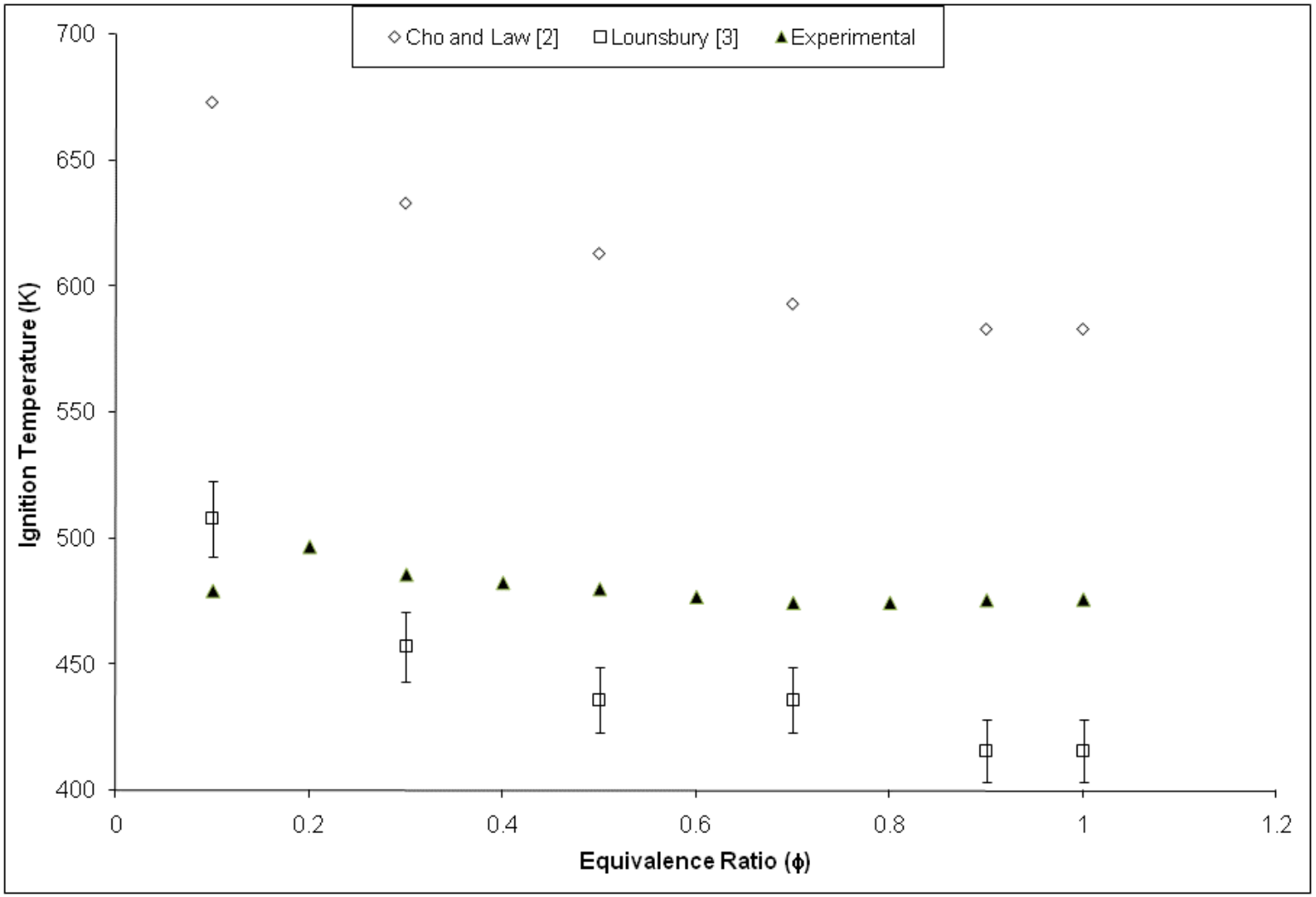


**Figure 3-13: Equivalence ratio vs. $T_{ig}$ comparison at 7.5% fixed volume of oxygen.**

## 3.3 Effect of Water Addition

One of the main objectives of this study was to research the effects of adding water vapor to the reactive mixtures. Figure 3-12 and Figure 3-13 compare the ignition temperatures of dry mixtures with those for increasing amounts of water vapor content for a fixed propane and a fixed oxygen amount. Both these figures clearly illustrate that as the water content is increased, the ignition temperature, and consequently the power required to initiate reactions, increases. Although not all the data sets displayed this as obviously, it was definitely a noticeable overall trend.

For the surface reaction energy generation, there wasn't any apparent difference caused by the addition of water vapor. Figure 3-12 shows the results for the 1.5% fixed volume propane set, and it can be seen that in this case the energy generation increases with the addition of water vapor. The 1.0% fixed propane showed similar results, however, the 2.0% fixed propane set showed the opposite, a decrease in energy generation with water addition. The fixed volume oxygen sets all had similar results to the 12.5% set shown in Figure 3-13, where all the data basically collapsed on itself. For both the fixed volume propane and oxygen sets, any difference that was seen with water addition was less than 0.3 W and more commonly was about 0.1 W.

These results of higher ignition temperatures and almost no change in energy generation with the addition of water imply the water has no chemical effect on the reactions; it is merely inhibiting the initiation of surface reactions. This inhibition could be due to water molecules occupying sites on the platinum wire surface or because water has a high specific heat capacity, thus more thermal energy is required to initiate the reactions. Dissociation of water on the surface and desorption of OH radicals into the gas phase, Deutschmann [17], to aid combustion ignition is theoretically possible but not studied here. The data suggests the surface reactions are not affected by water in the mixture once they are initiated.

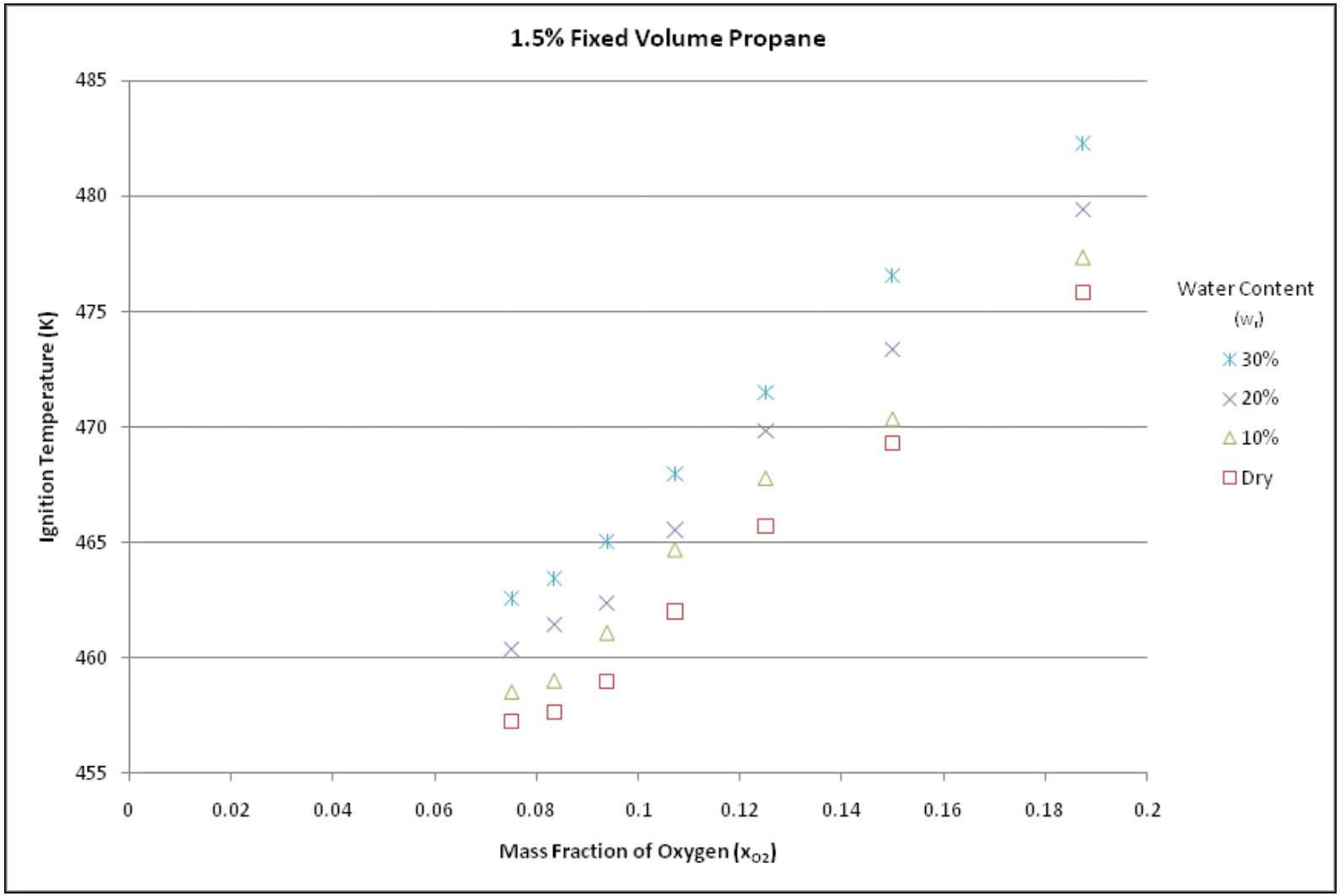


**Figure 3-14: Impact of water on $T_{ign}$ for 1.5% fixed volume propane.**

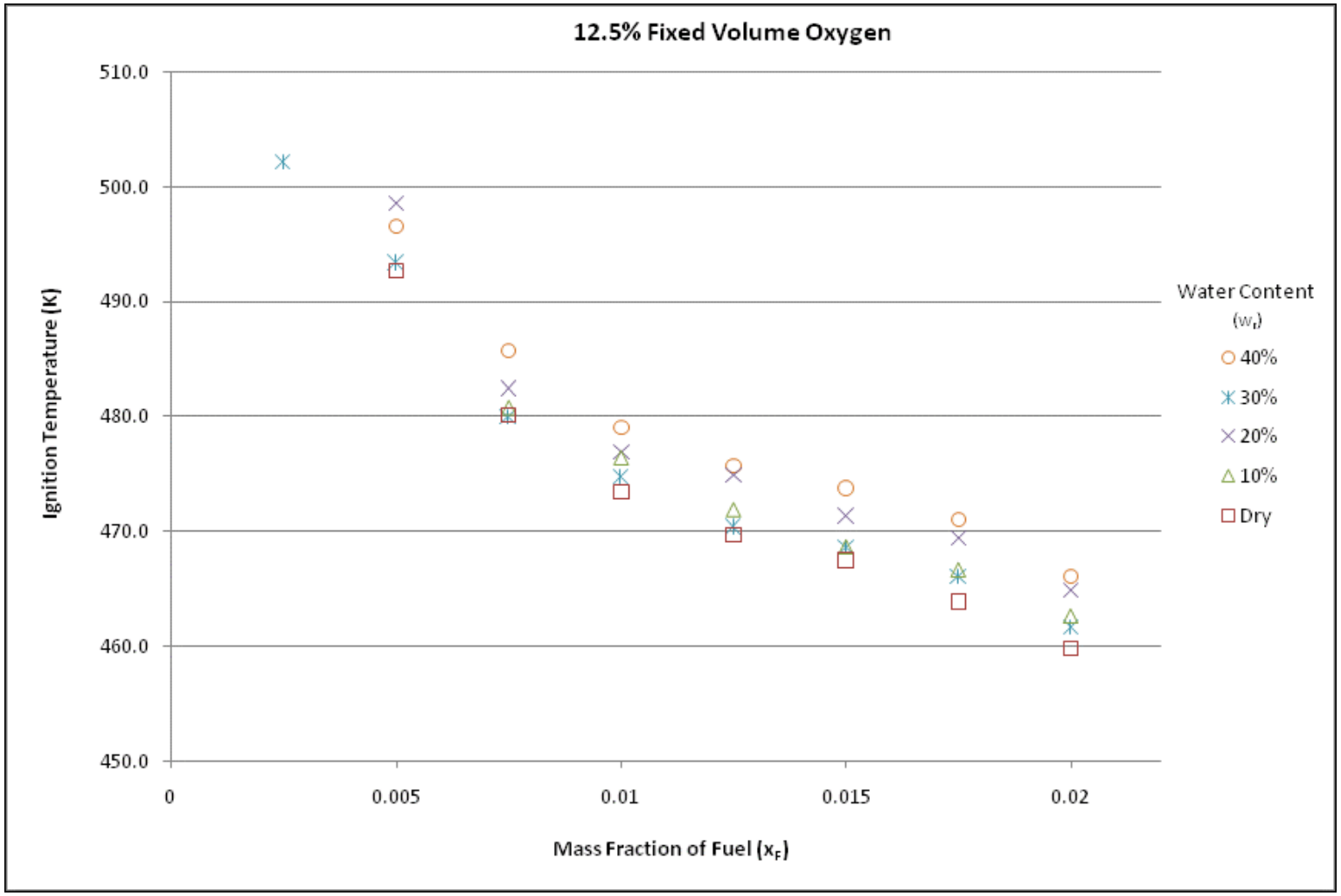


**Figure 3-15: Impact of water on $T_{ign}$ for 12.5% fixed volume oxygen.**

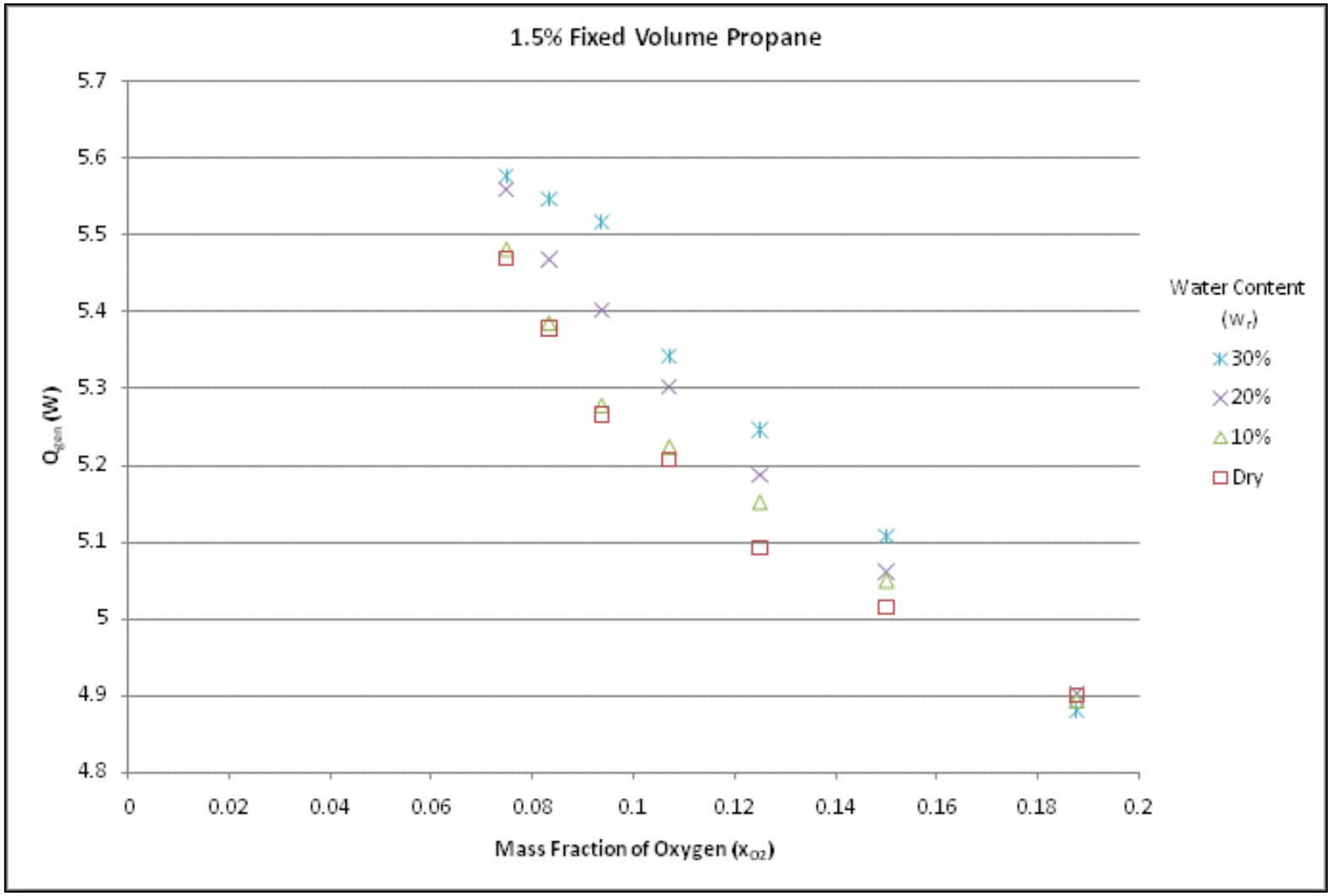


**Figure 3-16: Impact of water on $Q_{gen}$ for 1.5% fixed volume propane.**

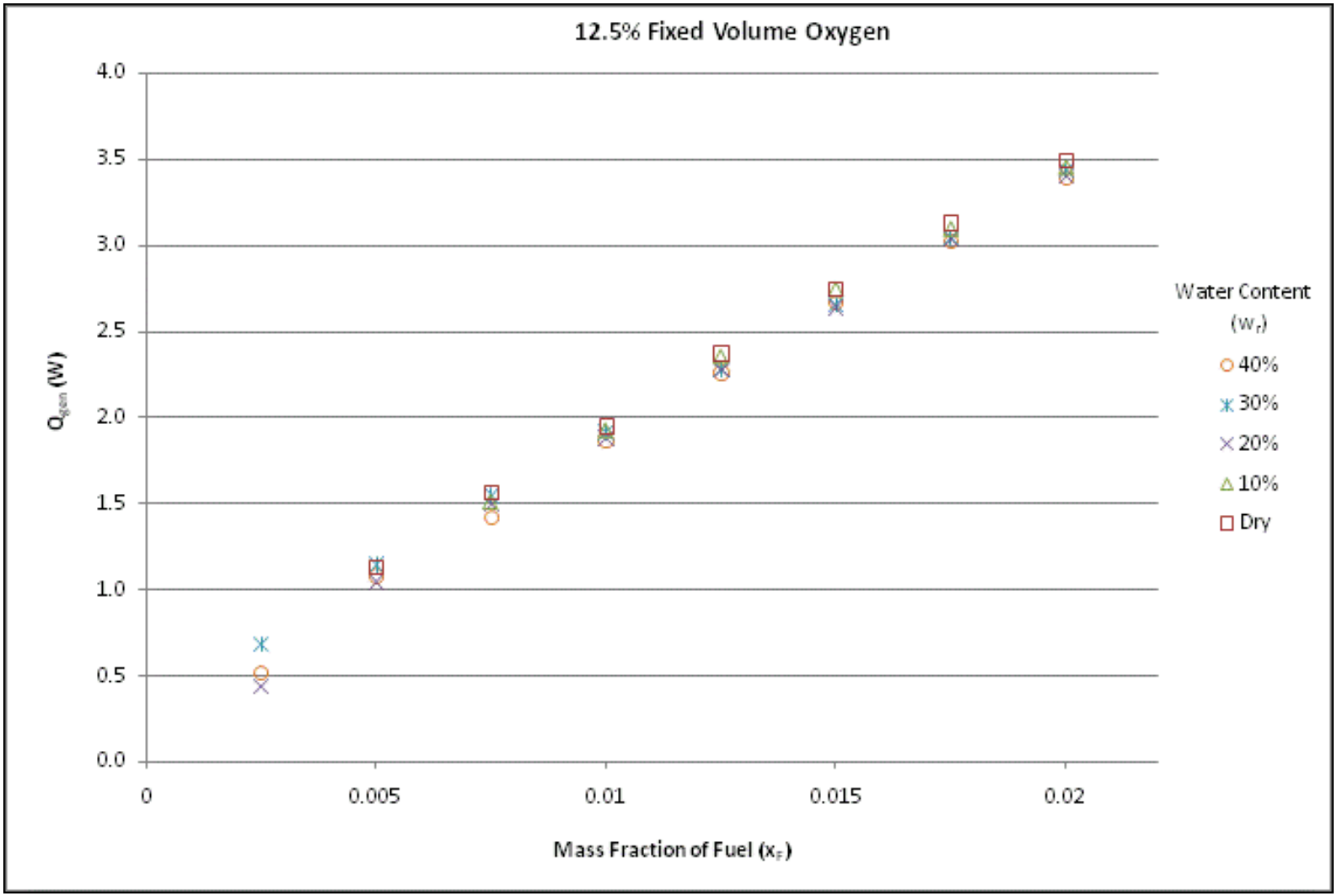


**Figure 3-17: Impact of water on $Q_{gen}$ for 12.5% fixed volume oxygen.**

The effect on ignition temperature and energy generation the water addition to the fuel has is important to the CPT igniter design. This information will be useful during future experiments of ethanol and water mixtures over the platinum wire. From Figure 3-12 and Figure 3-13, it is clear that generally the ignition temperature increases with water addition to the mixture. Although this trend is fairly obvious in these two figures, it was much clearer in the fixed volume propane experiments than in the fixed volume oxygen ones. This is most likely because the amount of water in the mixture is constant for $0.1 \leq \varphi \leq 1.0$ during the fixed propane experiments, and has to be changed using the process diagramed in Figure 2-4 at each equivalence ratio during the fixed oxygen experiments. Therefore, the additional time to adjust the water flow rate and wait until it reaches steady-state between the experiments may cause discrepancies, or the flow rates may not become as steady while changing them more often. However, the charts summarizing ignition temperature and energy generation results for the dry experiments, Figure 3-7 through Figure 3-10, also show much more distinct trends for constant propane than constant oxygen. This may suggest that the data is more consistent with higher amounts of propane in the mixture, or it could also be possible that the data taken earlier on during experimentation was more consistent.

When adding water to the mixtures, it became apparent that the experimental set up could only evaporate approximately 1000 $^{\mu L}/_{hr}$ steadily. Figure 2-6 shows a typical output from the dew point monitor. The curves from below 1000 $^{\mu L}/_{hr}$ are essentially linear, where as those above are not linear at times. The variable voltage supplies were used to increase the preheated nitrogen temperature as the water flow rate was increased to maintain steady-state. However, above the 1000 $^{\mu L}/_{hr}$ the balance of pre-heat temperature and water flow rate wasn't easily found. This could have been due to reaching the boiling point of water in the sintered metal filter or possible flooding of the filter, in which case a higher capacity filter may be a solution. At 1000 $^{\mu L}/_{hr}$ the variable voltage supplies were both set to 70, which corresponded to 70% of the maximum output for the heat tape. Therefore, above 1000 $^{\mu L}/_{hr}$ the issue causing unsteady flow was most likely not caused by inadequate heating of the nitrogen stream. Readings from the thermocouple in the nitrogen stream show it begins to reach 100 °C, the boiling point of water, with the rheostats set above 70. Future work evaporating ethanol-water mixtures from the syringe pump will show if it is possible to again reach steady-state flow above the boiling point of the mixture.

# 4 Heat Transfer Modeling

Throughout the course of this research, a number of models were explored to further understand the physics and chemistry of the system. The heat transfer from the electrically heated wire to the air stream was modeled using Fluent®, computational fluid dynamics software that uses finite volume analysis. A partial differential equation analysis was applied to model the heat transfer as well. These models accounted for diffusion along the length of the wire, convection from the wire to the air stream, radiation from the wire, and a source term for energy generation within the wire.

## 4.1 Fluent® Finite Volume Analysis

Fluent® was used to run a finite volume analysis of the platinum coil in cross-flow. This model may be helpful in the future for predicting the average wire temperature of the catalyst. For this study, the Fluent® model was only used to explore the average wire temperature as a function of power input for non-reactive flows, the 'Air' curve in Figure 3-1 through Figure 3-4. In the future, this model will be extended to predict ignition and reaction properties when it is integrated with Chemkin®.

### 4.1.1 Methods

***Governing Equations***

The Navier-Stokes momentum equation, shown as Equation 4.1, the continuity equation, shown as Equation 4.2, and the energy balance, shown as Equation 4.3, from [18] were used as the governing equations. The boundary conditions for these equations can be described with the Fluent® settings. The model was set to inviscid flow creating the plug-flow within the quartz tube. This gave a shear stress equal to zero at the quartz tube walls. However, the shear stress was accounted for along the coil walls; the velocity at the coil surface equaled zero. An energy balance was performed at the interface of the fluid and the coil wall. At this point, the energy generated within the coil has to equal the energy transferred to the surroundings by conduction, convection, and radiation. The temperature boundary conditions used included setting the ends of the wire at a fixed temperature, and then due to symmetry, the change in temperature with respect to x along the coil length would be zero at the

midpoint. Lastly, the temperature of the fluid was assumed to approach free-stream temperature, 293 K, at the edge of the thermal boundary layer around the coil.

$$\rho \frac{D\vec{v}}{Dt} = \rho g - \vec{\nabla} p + \mu \vec{\nabla}^2 \vec{v}$$ **Equation 4.1**

$$\vec{\nabla} \cdot \vec{v} = 0$$ **Equation 4.2**

$$\rho \frac{DU}{Dt} = \vec{\nabla}\left(k\vec{\nabla}T\right) + \frac{Dp}{Dt} + \Phi$$ **Equation 4.3**

### *Drawing and Meshing*

Two models were run using Fluent®: 1) a preliminary model; and 2) a more detailed model with more accurate radiation parameters. The preliminary model geometry included the wire and air only, with the wire modeled as a blackbody. The more detailed modeled also included the quartz tube, but the change that affected the model most was including the emissivity of platinum which is dependent on temperature. For each model, a SolidWorks® drawing of the coil and quartz tube configuration was made. The first included a 127 micron diameter coil having a total length of 13.208 cm. The air volume around the coil was also included, with a diameter of 2.7305 cm, the inside diameter of the quartz tube. The second drawing was similar, but included the quartz tube with a 3.29 cm outside diameter, as well as longer wire ends to represent the entire 14.224 cm of coil between the lead clips. Once these drawings were complete, they were imported into Gambit® to be meshed. The meshes were created by first meshing the edges, then surfaces, and finally the volumes. This was to ensure there was a fine enough grid at the critical points around the wire to produce accurate results. Figure 4-1 shows the coil in the quartz tube; the intensity of the glowing wire overwhelms the camera. The meshed drawings can be seen in Figure 4-2 and Figure 4-3.

**Figure 4-1: Platinum coil in the quartz tube, glowing from electrical heating.**

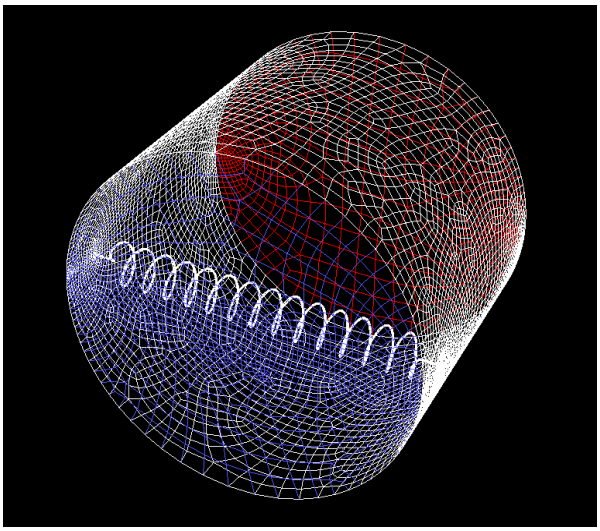

**Figure 4-2: Gambit® mesh for preliminary model, 237,107 elements.**

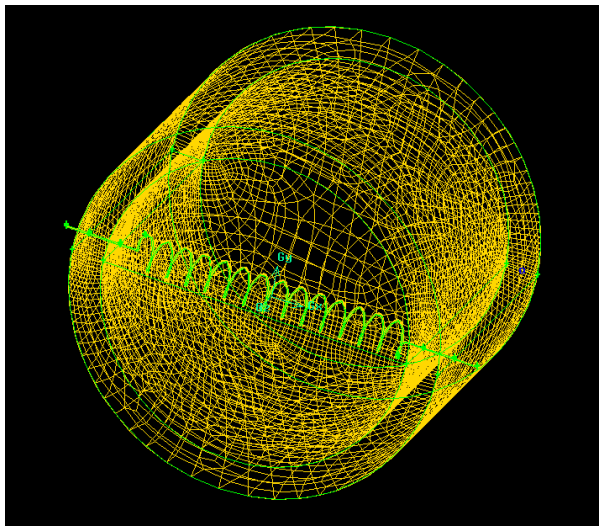

**Figure 4-3: Gambit® mesh for detailed model, 312,189 elements.**

### *Preprocessing and Solver Parameters*

Next, the materials and boundary conditions were defined in Fluent®. For the preliminary model, platinum had to be added to the database by inputting values for density, specific heat, and thermal conductivity. Air was already defined as a material; however, it was found that the results became much closer to those found experimentally once the specific heat and thermal conductivity of air were input as functions of temperature. For the more detailed

model, radiation properties had to be input for each material. These properties included absorption coefficient, scattering coefficient, scattering phase function, and refractive index. For all three materials platinum, quartz, and air, the scattering phase function was left as isotropic, the default selection. For platinum, an opaque solid, and air, a non-participating media, the absorption and scattering coefficients can be assumed to equal zero. Quartz is semi-transparent but spectral variation in absorptivity cannot be specified in Fluent®. Therefore, the model was run with the properties of quartz set at the extremes of being either transparent or opaque; the results only differed by 0.01 K. Lastly, the index of refraction, n, was entered for each of the materials as 2.33, 1.46, and 1 for platinum, quartz, and air respectively. The material property inputs for air, platinum, and quartz are summarized in Table 4.1.

Boundary conditions were set for each of the faces as well as all volumes (Table 4.2). The velocity of the air was set on the inlet face, with a value of 0.173 $^{m}/_{s}$ and a temperature of 290 K with the outlet set as outflow. The coil wall face was given a no slip boundary condition, as well as an emissivity. This emissivity varies with temperature, so it is chosen using the average wire temperature expected from the experimental results. A curve was calculated using emissivity data from a literature search [19 -26]. The resulting piece-wise function is shown in Equation 4.4.

Platinum emissivity as a function of temperature:

<u>For T < 582 K:</u>

$$\varepsilon = 1.65 \times 10^{-4}T - 1.6378 \times 10^{-2}$$

<u>For T > 582 K:</u>

$$\varepsilon = -5.23 \times 10^{-8}T^{2} + 2.34 \times 10^{-4}T - 3.84 \times 10^{-2}$$

**Equation 4.4**

All remaining faces were set as walls with zero shear stress on the air flow. The quartz tube faces were each given an emissivity of 0.93. The ends of the wire were fixed to remain at 290 K, due to the thermal inertia from the relatively large metal clips on the power supply leads. Each volume was set to participate in radiation, and finally the coil was given a source term to account for internal energy generation. All these boundary condition settings are summarized in Table 4.2.

**Table 4.1: Summary of Material Property Settings**

| Property | Air | Platinum | Quartz |
|---|---|---|---|
| Density ($^{kg}/_{m^3}$) | 1.225 | 21,450 | 2,620 |
| Specific Heat ($^{J}/_{kg\text{-}K}$) | $-0.365T + 8.5 \times 10^{-4}T^2 - 3.7 \times 10^{-7}T^3$ | 130 | 830 |
| Thermal Conductivity ($^{W}/_{m\text{-}K}$) | $3 \times 10^{-4} + 1.02 \times 10^{-4}T - 4.86 \times 10^{-8}T^2 - 1.52 \times 10^{-11}T^3$ | 71.6 | 1.46 |
| Viscosity ($^{kg}/_{m\text{-}s}$) | 1.789E-05 | -- | -- |
| Absorption Coefficient ($^{1}/_{m}$) | -- | 1 | 4.5 |
| Index of refraction | 1 | 2.33 | 1.46 |

**Table 4.2: Summary of Boundary Condition Settings**

| Boundary Conditions | | Setting | Comments |
|---|---|---|---|
| Face | Inlet | Velocity=0.173 $^{m}/_{s}$ | Calculated from volume flow rate and area of opening in quartz-tube. |
| | Outlet | Outflow | Flow exit with unknown pressures and velocities. |
| | Coil Wall | No Slip[1] | To account for boundary layer on coil. |
| | | ε(T)=0.117[1] | Emissivity of platinum set according to expected average temperature. |
| | Tube in | Shear stress=0 | To account for plug-flow. |
| | | ε=0.93[1] | Emissivity of quartz. |
| | | Semi-transparent[1] | For radiation model. |
| | Inlet and Coil Ends | T=290 K | The inlet air flow is at room temperature, and the coil ends are fixed at room temperature to account for effects of the large lead clips. |
| Volume | Coil | Source Term | Input in $^{W}/_{m^3}$ to account for electrical heating of the coil. |
| | Air | Participates in Radiation | Includes radiation as a form of heat transfer. |
| | Quartz Tube | Participates in Radiation[1] | Includes radiation as a form of heat transfer. |

[1] A setting was changed from the preliminary model.

**Table 4.3: Summary of Model Settings**

| Model | Settings | Comments |
|---|---|---|
| **Solver** | Pressure-based | Inlet velocity is due to a pressure gradient. |
| | 3D | Model drawing is 3-dimentional. |
| | Steady-state | During experiments, changes in electrical resistance were not recorded until they had stabilized at a steady state. |
| | Implicit | Unknown temperature in each cell is dependent on unknown temperature of neighboring cells. |
| **Energy Equation** | On | Heat transfer is the main area of interest. |
| **Radiation** | Discrete ordinates | Solves radiative transfer equation for a finite number of discrete solid angles, for radiation heat transfer from the coil to air. |
| **Viscous** | Laminar | Re is extremely low in this application, less than 1 if calculated as a cylinder in cross-flow using wire diameter as characteristic length; laminar is the most appropriate option available. See discussion below. |

With the boundary conditions input, the next step was to determine which models and restrictions should be applied. These are summarized in Table 4.3. The solver model was set to pressure-based, 3D, steady-state, and implicit and the energy was set to run due to the heat transfer. The radiation model was set to run using discrete ordinates to account for the radiation heat transfer from the wire to the environment. Lastly, the viscous model was set to run for laminar flow, which was the best choice available for the low Reynolds number flow. The laminar flow setting coupled with all walls, except the coil wall, set to have zero shear stress was the best method to emulate the plug flow within the quartz tube. The upstream velocity profiles in Fluent® represent perfect plug flow as shown in Figure 4-4. Downstream of the flow disturbance due to the coil, the velocity remains fairly uniform across the diameter of the quartz tube. For comparison, velocity profiles measured with a hot-wire anemometer in the quartz tube are plotted in Figure 4-5. Figure 4-5 shows flat profiles

±13.8% across the diameter of the tube where the coil is located, similar to those shown in Figure 4-4 that were calculated with Fluent®.

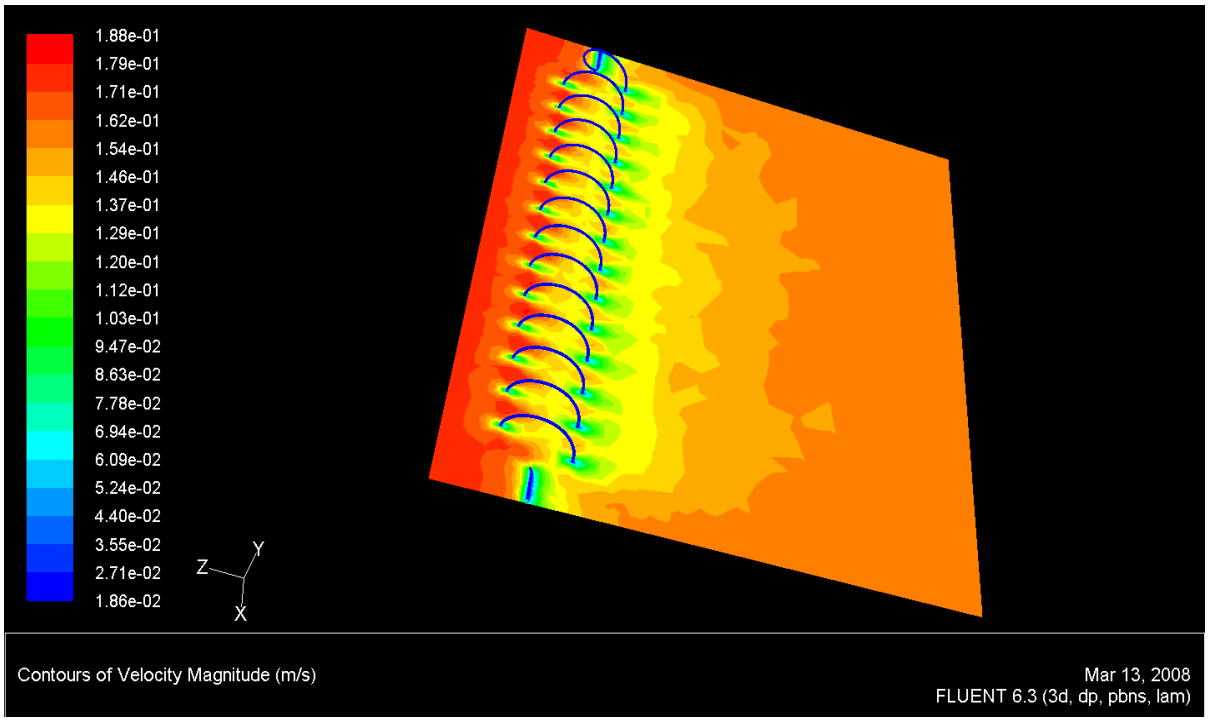


**Figure 4-4: Fluent® velocity contours around the electrically heated platinum coil.**

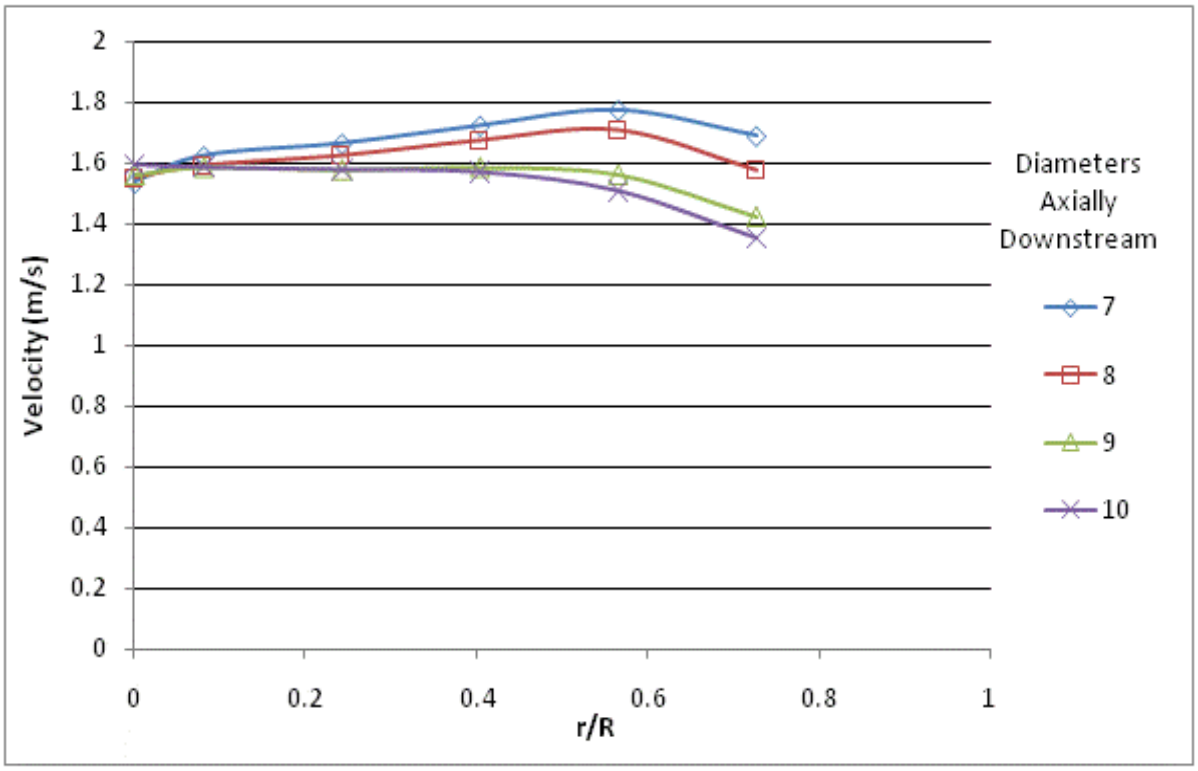


**Figure 4-5: Velocity profiles near the coil measured with a hot-wire anemometer.**

### 4.1.2 Results

For each model, the program was run with a source term accounting for a power input of 1 W up to 11 W at 1 W increments. At each power input value, the temperature contours could be displayed, temperature as a function of position along the coil could be plotted, and the average temperature was reported. The temperature contours and plot for a power input of 9 W from the preliminary model are shown in Figure 4-6 and Figure 4-7. The contour plots are useful to verify the model is working correctly, and the heat is being transferred downstream as expected. The temperature vs. position plot is important when we consider points of ignition and kinetics because it shows the temperature range along the wire. This plot also shows that the leading sides of the coil are at lower temperatures than the sides. The ends of the coil are maintained at room temperature as set by the boundary conditions in Fluent®.

These plots, along with plots such as velocity and pressure plots that are available, are useful in determining if the models and parameters were defined correctly. However, the most useful output from Fluent® for the purpose in this study is the volume average integral

report. This report provides the average wire temperature calculated by taking a weighted average by volume of the temperatures of the coil's mesh elements. This temperature is comparable to the average temperature found experimentally, and a plot of these results for both the Fluent® preliminary and detailed model is shown in Figure 4-8.

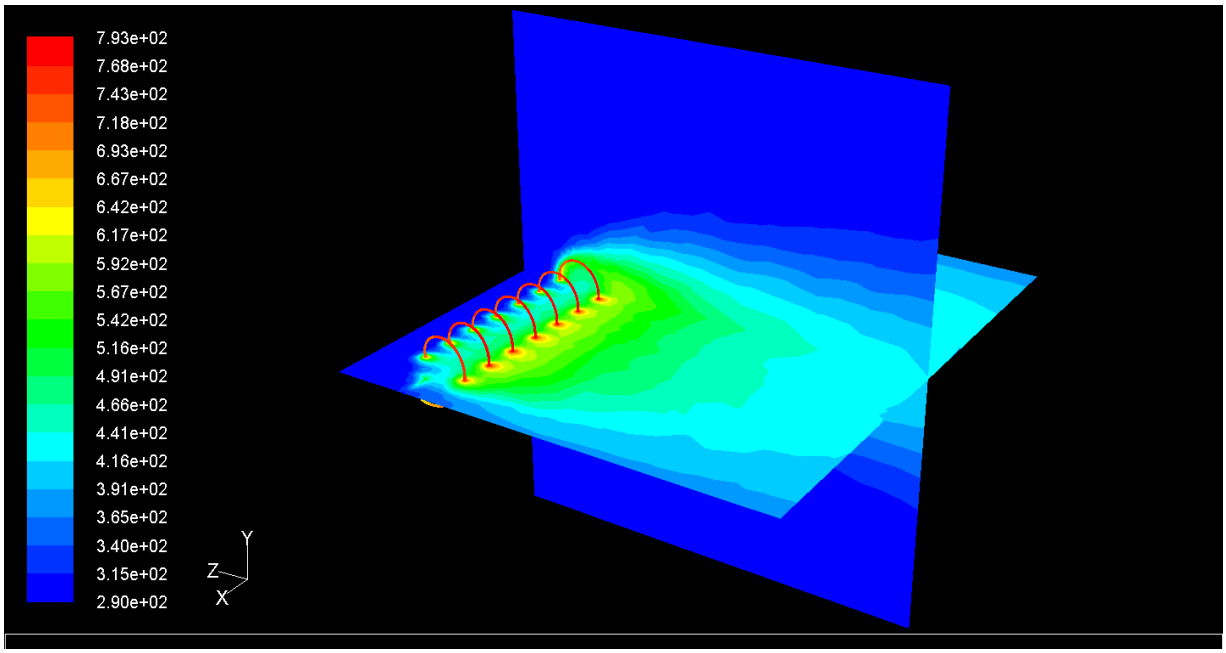


**Figure 4-6: Coiled wire and flow temperature contours with power set to 9 W.**

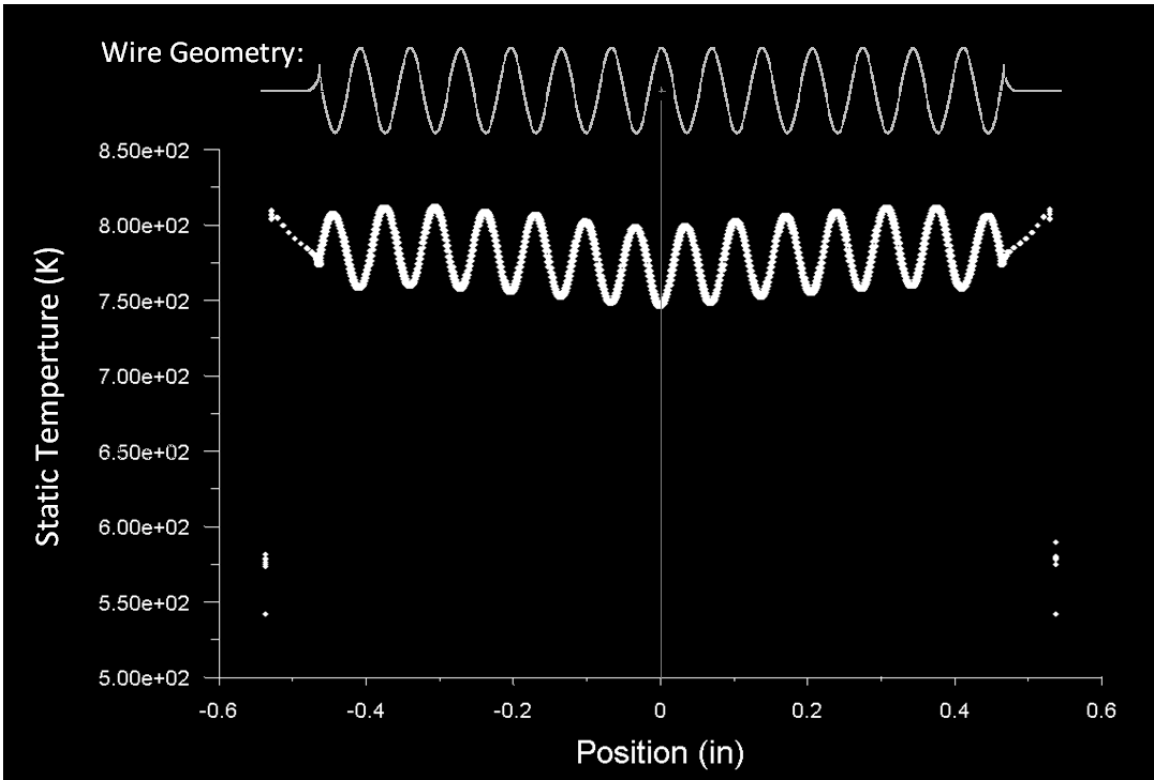


**Figure 4-7: Temperature distribution of the coiled wire with power set to 9 W.**

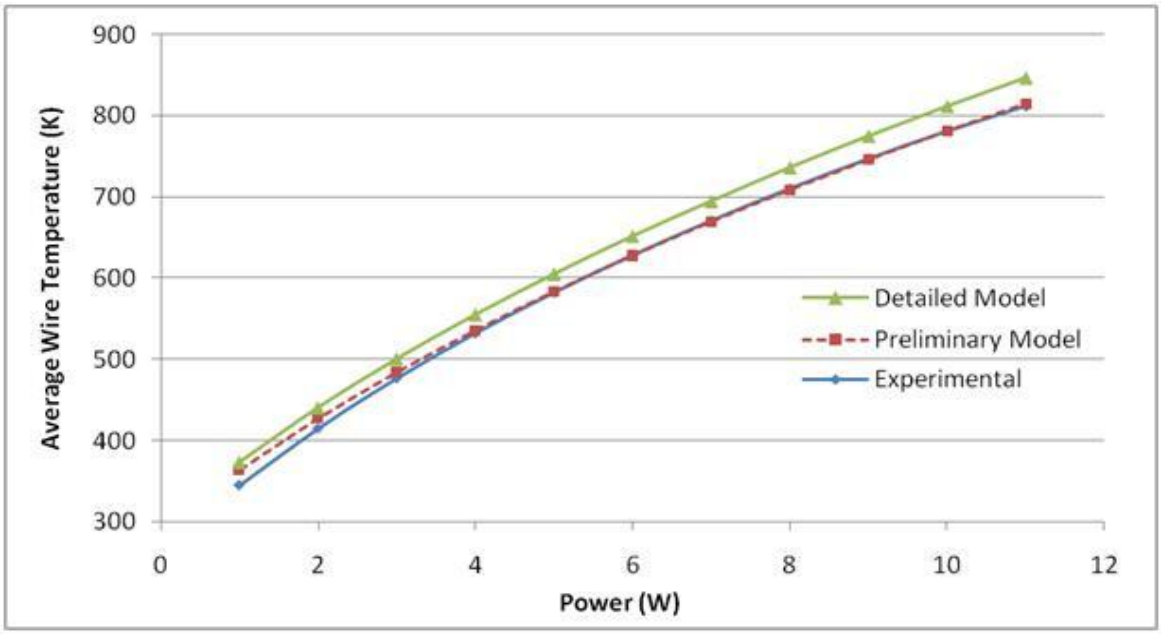


**Figure 4-8: Experimental data with Fluent® preliminary and detailed model results.**

From Figure 4-8, it is clear that the temperature difference between the experimental values and the preliminary model increases at low power inputs. The detailed model was run to try to explain the discrepancies at lower temperatures. It can be seen that the overall error between the detailed model and the experimental values is greater than the error between the preliminary model to the experimental data; however the detailed model has a constant offset of about 26.3 K ± 3.64 K. These results are discussed further in Section 4.3.

## 4.2 Partial Differential Equation Model

A partial differential equation was also derived and solved to model the platinum wire in cross-flow of non-reacting flows. The goal of this was to better understand the system overall, but also to use the results to improve the Fluent® model. Therefore, the analytical model was created using the same settings, boundary conditions, and model parameter-type inputs as were entered into Fluent®. However, there were some major exceptions to creating an environment with the same settings. First, the Fluent® model is using the actual coiled geometry where the analytical model assumes a straight cylinder. Second, the quartz tube is included in the Fluent® model but is not part of the analytical. In addition, the analytical model assumes air-flow over the entire length of the wire whereas the Fluent® model accounts for the approximately 5 mm at the ends of the wire between the lead-clips and where the air-flow reaches the wire. Finally, an assumption was included in the analytical model that temperature within a cross section of the wire is not dependent on radial position, a reasonable assumption considering the wire diameter is only 127 μm. Exploring the Fluent® mesh model revealed that it only includes six nodes around the wire and none inside its volume, so it makes a similar assumption.

Keeping these assumptions in mind Equation 4.5 was derived; a transient heat equation that includes diffusion along the platinum wire, convection and radiation carrying heat from the wire, and a source term for energy generation within the wire. Equation 4.6 is a version of Equation 4.5 with condensed coefficients, where $\alpha$, $\beta$, and $\gamma$ are calculated from material properties of platinum and air. The ST constant is multiplied by $(1-e^{-t})$ so that the power input is zero initially, and reaches 100% within a few seconds. The boundary conditions fix the ends of the wire at room temperature, and the initial condition sets the entire length of the wire at room temperature to start.

**Equation 4.5**

$$\rho_{pt} C_{p_{pt}} \left(\frac{d}{dt} T\right) = \frac{d}{dx} k_{pt} \left(\frac{d}{dx} T\right) - A_w h(T - T_0) - A_w \sigma\varepsilon\left(T^4 - T_0{}^4\right) + \frac{P}{V}(1 - e^{-t})$$

$$T(0,t) = T_0 \qquad T(L,t) = T_0 \qquad T(x,0) = T_0$$

Where, $T_0$=293K L=142mm

$$T_t(x,t) = \alpha_d T_{xx}(x,t) - \beta[T(x,t) - T_0] - \gamma\left[T(x,t)^4 - T_0{}^4\right]$$

**Equation 4.6**

After multiple transformations of Equation 4.6, it was solved using eigenfunction expansion. These transforms can be seen in the step by step explanation of the entire process, including the calculation of the coefficients from Equation 4.6, in Leichliter [29]. Using the eigenfunction expansion, however, the non-linear radiation term proved difficult to include, so the equation was solved without it. To see how much the radiation term would affect the solution, Equation 4.6 was also solved including the radiation term with the MathCad® built-in function PdeSolve.

Both the eigenfunction expansion and PdeSolve methods gave very similar results. A 3-D temperature mesh as a function of time and position along the wire is shown in Figure 4-9. And from Figure 4-10, it can be seen that the PdeSolve, which included the radiation term, predicted slightly lower temperatures than the eigenfunction expansion at higher powers, which was expected. All the average temperatures as well as the percent contributions from radiation are presented in the Section 4.3 with a brief discussion of observations.

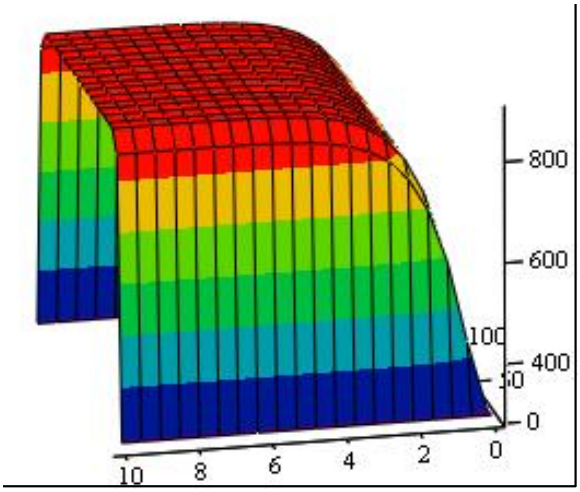


**Figure 4-9: 3-D mesh, temperature vs. time vs. position along wire.**

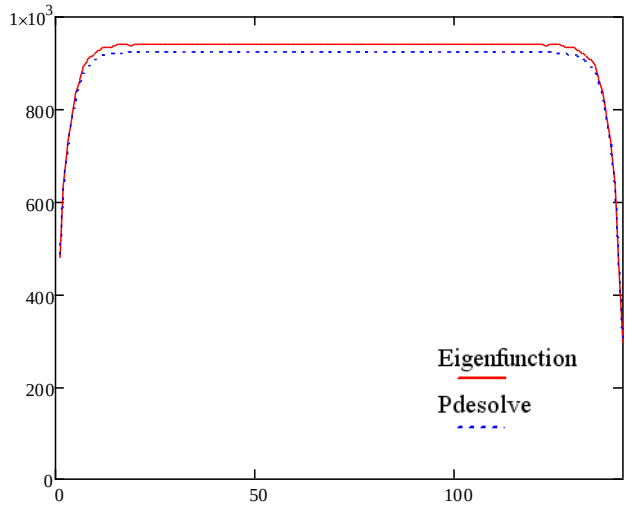


**Figure 4-10: Steady-state temperature profile along wire length.**

## 4.3 Results of Heat Transfer Modeling

After running the Fluent® model and solving the analytical partial differential equation model for a power input of 1-11 W at 1 W increments, the results were compiled and are shown and plotted in Table 4.4 and Figure 4-11. In Table 4.4, the second column, experimental data, refers to the data initially collected by Lounsbury [3]. The SourceMeter column is again experimental data but collected using the improved method from this study with the Keithley® SourceMeter. The next three columns contain the results of the detailed Fluent® model, the analytical model solved by eigenfunction expansion that neglects radiation affects, and the analytical model that includes a radiation term, solved using a MathCad® built-in function, PdeSolve. Finally, the percent radiation calculated by Fluent® and that calculated from the difference in the eigenfunction and PdeSolve results are displayed in the last two columns.

**Table 4.4: Average Temperature Experimental Data and Heat Transfer Models Results**

| Power Input (W) | Experimental Data [3] (K) | Source-meter (K) | Fluent® Model (K) | Eigen-function (K) | Pdesolve Model (K) | % Radiation Fluent® -- | % Radiation Pdesolve -- |
|---|---|---|---|---|---|---|---|
| 1 | 344.8 | 359.6 | 373.6 | 370 | 370 | 4.58 | 0.00 |
| 2 | 414.8 | 421.8 | 440.9 | 438 | 438 | 5.69 | 0.00 |
| 3 | 476.9 | 480.1 | 500.8 | 501 | 500 | 6.90 | 0.20 |
| 4 | 532.4 | 534.7 | 555.2 | 560 | 559 | 8.15 | 0.18 |
| 5 | 582.6 | 586.0 | 605.3 | 616 | 614 | 9.44 | 0.33 |
| 6 | 628.7 | 634.2 | 651.9 | 670 | 666 | 10.71 | 0.60 |
| 7 | 671.2 | 679.6 | 695.5 | 722 | 717 | 11.99 | 0.70 |
| 8 | 710.8 | 722.6 | 736.4 | 772 | 765 | 13.26 | 0.92 |
| 9 | 747.6 | 763.4 | 775.1 | 821 | 811 | 14.50 | 1.23 |
| 10 | 781.5 | 802.2 | 811.8 | 868 | 856 | 15.73 | 1.40 |
| 11 | 812.4 | 839.5 | 846.7 | 915 | 900 | 16.93 | 1.67 |

From Table 4.4 and Figure 4-11, it is clear that the analytical method shows fairly good agreement to the Fluent® model and the experimental data. The discrepancies between the models increase at higher power inputs, with the Fluent® model predicting slightly higher temperatures that the experimental data, and the analytical models predicting even higher. The eigenfunction method predicted the highest temperatures, about 75 K, or 9%, too high at 11 W. One sure cause of this is that radiation was not accounted for in the eigenfunction expansion model. Since it was included in the Pdesolve method, after comparing the two, it

can be seen that the radiation term does improve the prediction by lowering it slightly, and at 11 W this difference is about 15 K or about 1.7%. This was interesting because the percent of heat transfer due to radiation can also be calculated in Fluent®, which claimed a max of 16.9% radiation at 11 W. Another factor that would likely cause inconsistencies is the geometry. To include the coiled geometry in the analytical models, the convection coefficient h would have to be calculated for a coil. This would suggest a periodic h dependent on position along the wire. Aside from the geometry, the method for calculating h would also affect the results. For the analytical model, Equation 4.7 was used, and with Fluent® the velocity of the air flow is entered, and it calculates h for each finite element. Considering these methods for improving the PDEs, the models seem to be fairly accurate, and a good tool for modeling the system.

$$h = \frac{Nu \cdot k_{air}}{D}$$ **Equation 4.7**

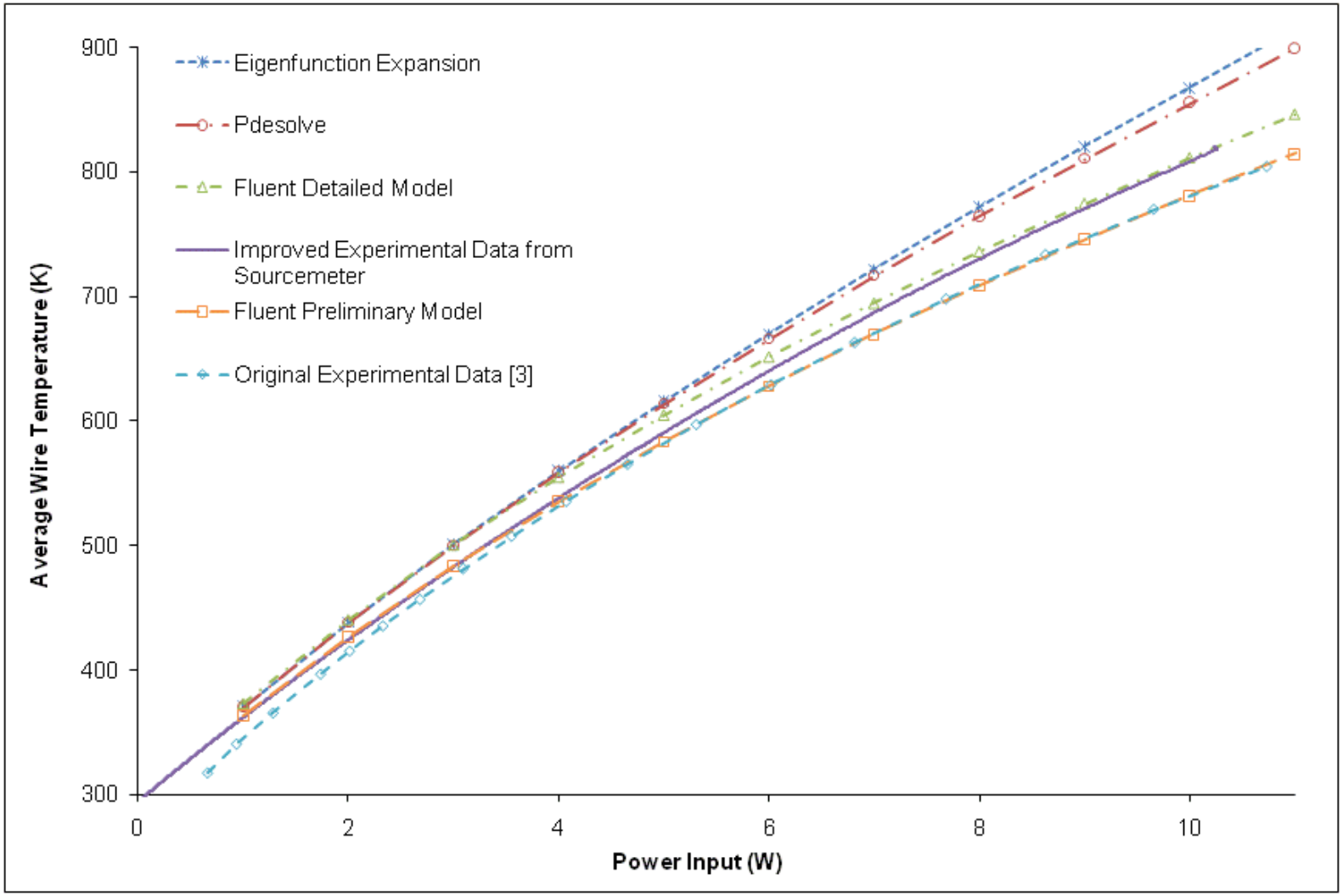


**Figure 4-11: Summary of experimental data and results from the Fluent® and PDE models.**

# 5 Conclusions and Future Work

## 5.1 Conclusions

The experiments in this work showed improvements over previous work by following some suggestions outlined by Lounsbury in [3]. The purchase of the Keithley® SourceMeter gave much greater control over the power input, which could be computer automated along with the resistance readings from the same device. The gas flow-rates were also controlled and validated automatically using LabView®. All manual settings and adjustments were eliminated, making the experiments much more repeatable as well as greatly improving the quality of the data. With more fine-tuned data, the one-step Perger model could be improved merely due to more data points available for curve-fitting. Water was also injected into the gas stream as a progressive step in studying alternative transportation fuels, which may be in liquid form and may be mixed with water.

A tubular plug-flow reactor was used to study the interactions of non-flammable propane-oxygen-water mixtures diluted with nitrogen over a coiled platinum wire catalyst. The wire catalyst was electrically heated and the average wire temperature was calculated by measuring the electrical resistance of the wire and using the temperature coefficient of resistance for platinum. The average temperature of the wire was plotted as a function of the power input, and from these plots the temperature and power required to initiate surface reactions was determined. The heat release, or energy generated from the surface reactions, was also calculated from these plots. Heat transfer models were also applied to the system.

For each data set, generally, the ignition temperatures decreased and the heat release increased as the equivalence ratio increased. This was the expected trend also seen by Lounsbury [3] and Cho and Law [2] in previous work. The addition of water increased the power and ignition temperature necessary to initiate surface reactions, however, it did not seem to effect the energy generation from the reactions. This suggested the water did not have a chemical effect on the surface reactions; it merely inhibited the reactions from being initiated. This could be due to water molecules occupying sites on the platinum wire surface or because water has a high specific heat capacity, more thermal energy is required to initiate the reactions. The data implies the reactions are not affected by water in the mixture once they are initiated.

Both an analytical partial differential equation model as well as a Fluent® finite volume model was applied to the catalytic wire with air flow across it. These both resulted in average wire temperatures similar to those found experimentally as a function of power input. The Fluent® model will be useful in predicting ignition temperatures as well as heat release from the wire once the chemical kinetic program ChemKin® is incorporated into the models.

Overall, this study has given further insight into non-flammable, homogeneous, propane-oxygen-water-nitrogen mixtures over a platinum wire catalyst. From the fairly simple experimental setup, the following were determined:

- Power input to the catalyst necessary to initiate surface reactions
- Average wire temperature when surface reactions initiate
- Energy generation due to surface reactions
- The effect of water addition on the mixtures

## 5.2 Future Work

A few items that may prove beneficial to the continued study in this area:

- Extending experimental methodology used in this study to alternative transportation fuels
- Improving the evaporation process for higher flow rates and water/fuel mixtures
- Incorporating a gas chromatograph-mass spectrometer for validating steady state evaporation of fuels, analogous to the dew point monitor used in this study for detecting water vapor
- Further examination of the “seasoning” of the catalyst
- Examine ignition properties of a grain stabilized or wash coated wire
- Coupling Chemkin® with Fluent® to predict ignition temperatures and heat release
- Purchase a thermal imaging camera to get more detailed wire temperature data over the average wire temperature data used throughout this study

## 6 References

[1] Patel, A. J., *System Characterization and Catalytic Ignition of Propane-Air Mixtures in a Plug Flow Reactor*, Master's Thesis, University of Idaho, 2004.

[2] Cho, P. and Law, C. K., "Catalytic Ignition of Fuel/Oxygen/Nitrogen Mixtures over Platinum," *Combustion and Flame*, 66: 159-170, 1986.

[3] Lounsbury, B. L., *Catalytic Ignition Temperatures of Propane-Oxygen-Nitrogen Mixtures over Platinum*, Master's Thesis, University of Idaho, 2007.

[4] Cherry, M. A., and Elmore, C. L., "Timing Chamber Ignition Method and Apparatus," US Patent, 4,997,873, 1990.

[5] Cherry, M. A., Morrisset, R., and Beck, N., "Extending the Lean Limit with Mass-Timed Compression Ignition using a Plasma Torch," SAE Paper, 921556, 1992.

[6] Cherry, M. A., "Catalytic-Compression Timed Ignition," US Patent, 5,109,817, 1992.

[7] Morton, A. T., *Homogeneous Charge Combustion of Aqueous Ethanol in a High Compression Catalytic Engine*, Master's Thesis, University of Idaho, 2000.

[8] Clarke, E. S., *Characterization of Aqueous Ethanol Homogeneous Charge Catalytic Compression Ignition*, Master's Thesis, University of Idaho, 2001.

[9] Cordon, D. A., *Multi-fuel Platform and Test Protocols for Over-the-road Evaluation of Catalytic Engine Technology*, Master's Thesis, University of Idaho, 2002.

[10] Williams, J., *Steady-State Dynamometer Testing of a Passenger Van Comparing Operation on Gasoline and Aqueous Ethanol*, Master's Thesis, University of Idaho, 2006.

[11] Harper, M., *Aqueous Ethanol in a CFR Engine for Homogeneous Charge Catalytic Compression Ignition (HCCCI)*, Master's Thesis, University of Idaho, 2006.

[12] Anderson, E. K., *Engine Platform Development and Validation for Studying Homogeneous Charge Catalytic Combustion of Aqueous Fuel*, Master's Thesis, University of Idaho, 2009.

[13] Perger, T., Kovács, T., Turányi, T., and Treviño, C., "Determination of Adsorption and Desorption Parameters from Ignition Temperature Measurements in Catalytic Combustion Systems," *Journal of Physical Chemistry B*, B107(10):2262-2274, 2003.

[14] Perger, T., Kovács, T., Turányi, T., and Treviño, C., "Determination of the adsorption and desorption parameters for ethane and propene from measurements of the heterogeneous ignition temperature," *Combustion and Flame*, 142:107-116, 2005.

[15] Lewis, B., and von Elbe, G., *Combustion, Flames and Explosions of Gases*, Academic Press, 3rd ed., 1987.

[16] Holman, J. P., *Experimental Methods for Engineers*, McGraw-Hill, 2nd ed., 1971.

[17] Deutschmann, O., Schmidt, R., Benrendt, F., and Warnatz, J., "Numerical Modeling of Catalytic Ignition," Twenty-Sixth Symposium (International) on Combustion, The Combustion Institute, pp. 1747 - 1754, 1996.

[18] White, Frank M., *Viscous Fluid Flow*, McGraw-Hill, 3rd ed., 2006.

[19] Jain, S. C., Goel, T. C., Narayan, V., 1969, "Thermal Conductivity of Metals at High Temperature by the Jain and Krishnan Method III. Platinum," British Journal of Applied Physics, 2, pp. 109-113.

[20] Ohta, H., 1986, "New Transient Calorimetric Technique for Determining the Total Hemispherical Emissivity of Metals – An Application of Laser Flash Method," High Temperature Materials and Processes, 7, pp. 185-188.

[21] Davisson, C., Weeks, J. R., Jr., 1924, "The Relation between the Total Thermal Emissive Power of Metal and its Electrical Resistivity," Journal of the Optical Society of America, 8, pp. 581-604.

[22] Geiss., W., Physica, 5, pp. 203-207, 1925.

[23] Krishnan, K. S., and Jain, S. C., 1954, "Determination of Thermal Conductivities at High Temperatures," British Journal of Applied Physics, 5, pp. 426-430.

[24] Bradley, D., and Entwistle, A. G., 1961, "Determination of the Emissivity, for Total Radiation, of Small Diameter Platinum-10% Rhodium Wires in the Temperature Range 600 – 1450 ºC," British Journal of Applied Physics, 12, pp. 708-711.

[25] Goard, P. R. C., 1969, "Application of Hemispherical Surface Pyrometers to the Measurement of the Emissivity of Platinum (A Low-Emissivity Material)," Journal of Scientific Instruments, 2, pp. 109-113.

[26] Leichliter, K., Lounsbury, B., Steciak, J., Budwig, R., and Beyerlein, S., "Finite Element Model of a Heated wire Catalyst in Cross Flow," ASME Paper, 68922, 2008.

[27] Icropera, P., Frank, and DeWitt, P., David, 2002, Fundamentals of Heat and Mass Transfer. New York: John Wiley and Sons Publications.

[28] Farlow, Stanely J. Partial Differential Equations for Scientists and Engineers. New York: Dover Publications, 1993.

[29] Leichliter, K., 2009, *Catalytic Ignition Properties of Propane-Oxygen-Water-Nitrogen Mixtures over Platinum,* Master's Thesis, University of Idaho, 2009.